A STUDY OF BULK AMORPHOUS ALLOYS FORMED BY SOLID-STATE REACTION IN ELEMENTAL COMPOSITES

Thesis by

Michael Atzmon

In Partial Fulfillment of the Requirements

for the degree of

Doctor of Philosophy

California Institute of Technology

Pasadena, California

1986

(submitted 22 July 1985)

ACKNOWLEDGEMENTS

I would like to express my deep appreciation to Professor William L. Johnson for guiding me during my graduate work. His unsurpassed enthusiasm and physical insight were extremely valuable and stimulated my interest in science. Bill's positive attitude and constant encouragement made my work with him extremely pleasant. The new field of solid-state amorphization, of which this thesis is part, is a result of Bill's creativity.

I missed very much the presence of Professor Pol Duwez in the past months. Until he passed away, Professor Duwez was a constant inspiration to the members of Bill's group. We all appreciated his good nature and the interesting discussions which we had with him.

I wish to express my thanks to Dr. Karl Unruh for useful discussions, for his help concerning computers and for providing sputtered samples. Drs. Bruce Clemens and Art Williams provided much appreciated help during the early period of my work at Keck Laboratories. I enjoyed many useful and interesting discussions with Lowell Hazelton, who showed constant interest in my research and contributed valuable comments. Special thanks are due to Jennifer Goldstein for her help in proofreading this manuscript. I would also like to thank my fellow graduate students and the research fellows in Bill's group for the pleasant and stimulating environment, in which I spent over four years. I would like to acknowledge Angela Bressan for her secreterial and technical help during my stay at Caltech and for her support in preparing this thesis. Concetto Geremia deserves thanks for making the third floor of Keck Building the lively place it is, and for being helpful to every student far beyond his duty.

Finally, I wish to thank my parents for their constant support and encouragement.

The Rutherford backscattering spectroscopy experiments were performed by Yang Tse Cheng and Dr. Mark Van Rossum in Professor M.-A. Nicolet's laboratory. Drs. E. D. Gibson and J. D. Verhoeven provided the powder-made composite used for the present study.

The financial support of Northrop Corporation, Standard Oil Company, Aerojet General and the United States Department of Energy is acknowledged.

ABSTRACT

Bulk amorphous Zr- and Er- based alloys have been synthesized by solid-state reaction in elemental composites prepared by mechanical deformation. For the Er- based composites, complete amorphization was achieved by near- isothermal rolling near room temperature. The driving force for the reaction was found to be a large negative enthalpy of mixing between the constituent elements. Strain and interfacial energies have been estimated and found to modify the driving force only slightly. X-ray diffraction and differential scanning calorimetry have been used to characterize the structure and crystallization behavior of the alloys obtained. Comparison to corresponding amorphous alloys prepared by liquid quenching and sputtering gave good agreement.

The diffusion of Au in amorphous Au-Y and Au-La thin films produced by co-evaporation has been studied by means of X-ray diffraction and Rutherford backscattering. An estimated diffusion coefficient agrees with those obtained by other authors for diffusion of Au in several amorphous alloys. The results confirm that there can be bulk self-diffusion in an amorphous alloy without crystallization. Thus, one does not need to assume short-circuit diffusion during the growth of an amorphous phase by solid-state reaction.

TABLE OF CONTENTS

LIST OF FIGURES

page

Chapter 1

page

Chapter 2

Chapter 3

page

Chapter 4

1. INTRODUCTION AND BACKGROUND

1.1 INTRODUCTION

Oxide-based glasses have been known to mankind for thousands of years. The most familiar, SiO_2 is used extensively in everyday life. These glasses are obtained by cooling a liquid at moderate rates of several degrees per minute and bypassing crystallization. They form if the time scale for crystallization is considerably smaller than the cooling time. In the past decades, the development of rapid cooling methods has led to the discovery of metallic alloy glasses. These materials have been synthesized by rapid cooling from the melt at rates of about 10^6 degrees per second. Metallic glasses have generated considerable interest among scientists and engineers, from the standpoint of fundamental understanding as well as for practical applications, although the latter have been limited by the small external dimensions of the samples.

In the past three years, a completely new approach was developed for the synthesis of metallic glasses. It has also been based on the kinetics of competing processes, but instead of rapid cooling, it employed an isothermal solid- state reaction in a crystalline diffusion couple.

It has been the purpose of the present work to extend the diffusion- couple experiment to three dimensions, making possible the synthesis of amorphous alloys in bulk form. Stated simply, this extension is based on mixing fine powders of the components of the diffusion couple, thus having interfaces for diffusion throughout the bulk. In addition to possible practical applications, the samples obtained allowed new characterization techniques to be used and also a comparison of the new amorphous alloys with those prepared by conventional techniques.

In this chapter, the theoretical background will be given for the formation and structure of both conventional and solid- state reacted amorphous alloys. Chapter two describes the experimental procedures used. In the third chapter, the results obtained for solid- state reacted bulk alloys are presented and discussed. In Chapter four, experiments on reactions between crystalline and amorphous phases in bulk as well as in thin films are described, and implications for the understanding of solid- state reactions in general are discussed. Chapter five contains a summary and suggestions for future studies.

1.2 METALLIC GLASSES

The term "metallic glass" refers to a metallic alloy which lacks crystalline long-range order. Beyond a few nearest-neighbor shells, there are no correlations between the atomic positions. The glassy state is metastable, and the equilibrium state of a metal alloy is always crystalline. In this section, a review of the principles of the synthesis of metallic glasses is given, with an emphasis on the more novel method of solid- state reactions (SSR). The structure of amorphous materials will then be discussed, including methods for its determination by diffraction methods.

1.2.1 Rapid Quenching

The traditional methods for synthesizing metallic glasses are based on rapid cooling of an alloy from the vapor or melt to kinetically bypass the formation of crystalline compounds. The first amorphous alloy produced by vapor deposition was reported by Buckel and Hilsch[1.1] in 1954. Klement et al.[1.2] were the first to produce a metallic glass by rapid cooling from the melt. Their method was based on atomizing a liquid alloy and bringing it in contact with a copper plate kept at room temperature- the "gun" technique. It is illustrated in Fig. 1.1, together with further developments. An additional method of rapid cooling is laser quenching, in which a short laser pulse melts a layer on the surface of a solid, which is then cooled by heat transfer to the bulk.[1.5] Typical cooling rates achieved in rapid quenching are 10^4-10^7 deg/sec (10^{12} deg/sec for laser quenching). For vapor deposition, the cooling rates are estimated to range as high as 10^{13} °C/sec.[1.6]

The kinetics of rapid cooling are described schematically in a temperature- time- tranformation diagram (Fig. 1.2). The solid curve represents the time required to transform a small fraction (e.g., one percent) of an undercooled liquid into a crystalline phase, as a function of the temperature, under isothermal conditions. This function is affected by the thermodynamics and kinetics of the transformation. The thermodynamic driving force is the difference in the Gibbs free energy $\Delta G_{x,l}$ between the liquid and crystalline phases. It decreases monotonically as a function of the temperature and becomes zero at the melting point. The kinetic factors depend on atomic rearrangement involved in nucleating a new phase or on long-range diffusion necessary to create domains with the chemical composition of the resulting phases. Both processes are thermally activated and increase exponentially with the temperature. The general expression for a nucleation- limited transformation rate is given by:[1.8]

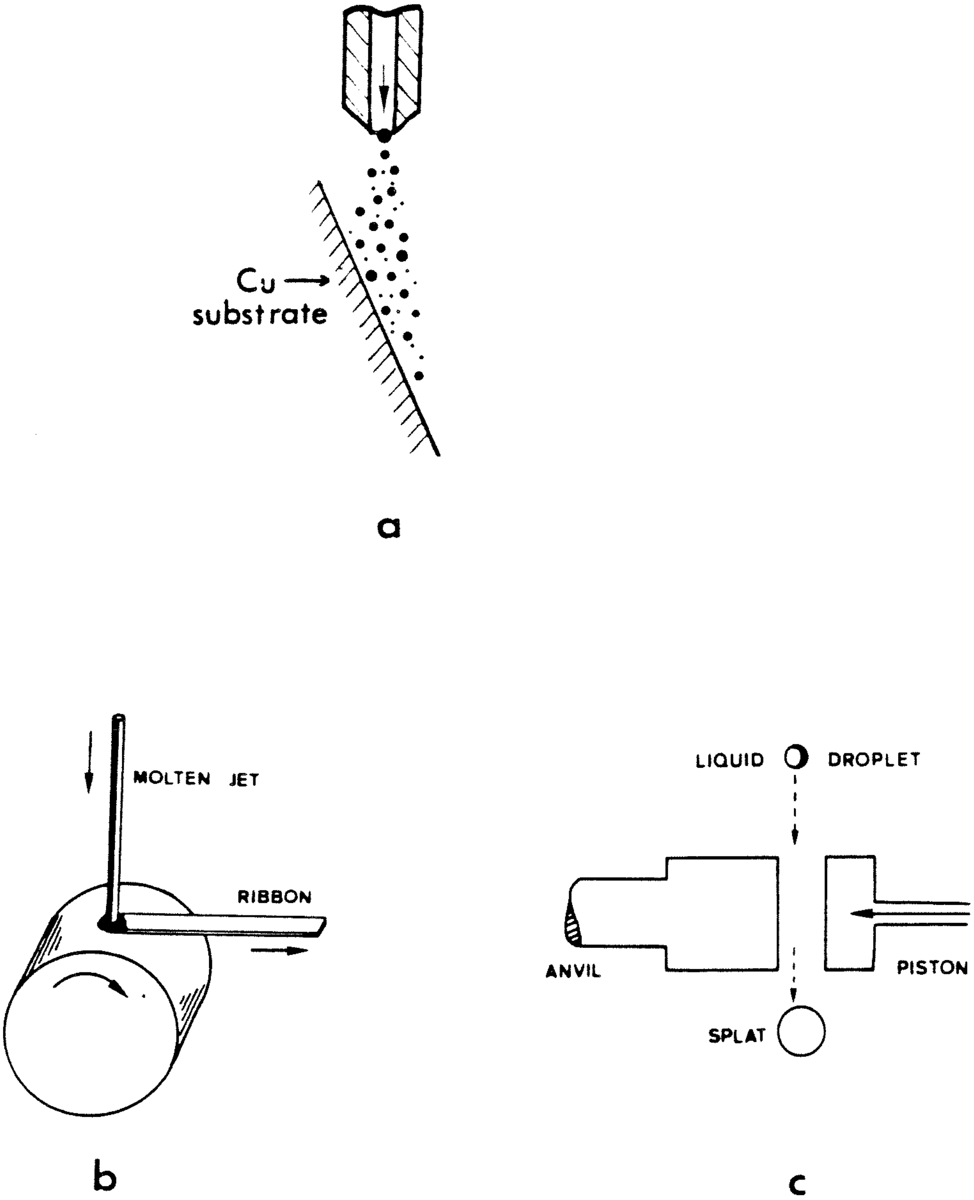

Figure 1.1 Three methods for rapid cooling of liquid alloys, a) "gun", b) meltspinning, c) piston and anvil (from Refs. 1.3,1.4).

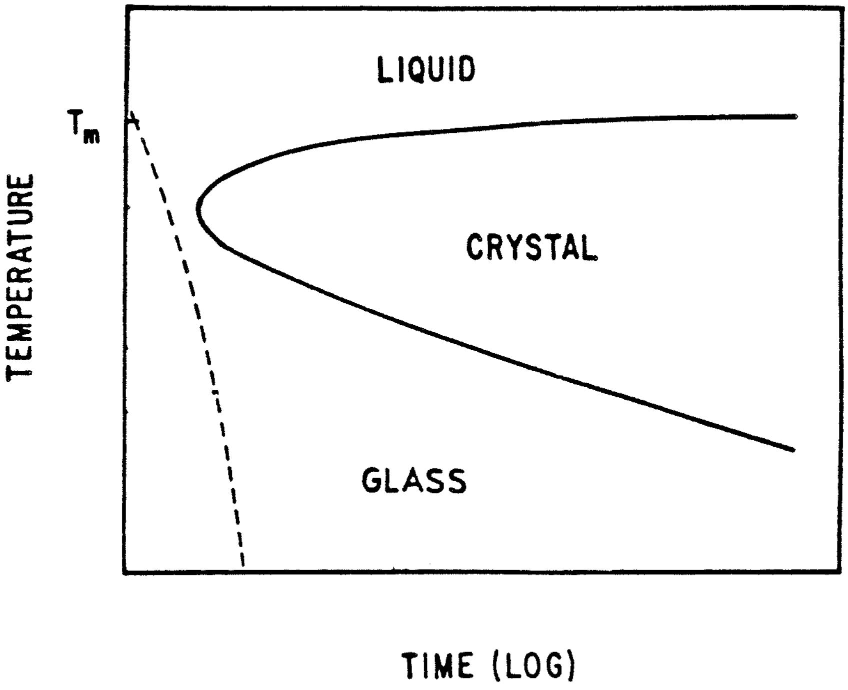

Figure 1.2 Schematic TTT diagram for crystal growth in an undercooled melt (from Ref. 1.7). T_m denotes the melting point.

$$I = N\nu \exp(-\Delta g_m/kT) \exp(-\Delta G_c/kT) \tag{1.1}$$

where N is the number of atoms per unit volume in the liquid phase and ν is a characteristic jump frequency. Δg_m is the activation energy for atomic migration and ΔG_c is the free energy associated with the formation of a critical nucleus. It depends on the driving force $\Delta g'$ through

$$\Delta G_c = 4\eta^3\sigma^3/27(\Delta g')^2 \tag{1.2}$$

where σ is the surface energy parameter and η is a geometrical factor depending on the shape of the nuclei. The competition between the thermodynamic and the kinetic factor gives the curve its nose-like shape. If we use this curve as an approximation for continuous cooling, one can see that there is a minimum cooling rate, as represented by the slope of the dotted line, necessary to bypass the formation of the crystalline phase.

Amorphous metal alloys are more stable and form more easily than elemental metals. For rapid quenching, the accessible range of composition is usually around deep eutectics in the binary phase diagram, as pointed out by Cohen and Turnbull.[1.9] This is only a kinetic constraint specific to rapid cooling from the melt. For vapor deposition, the range of compositions is far more extended. For pure elemental metals, an effective cooling rate of 10^{14} $^{\circ}$C/sec is necessary to form amorphous solids, and it can be achieved by deposition onto a substrate kept at 4 $^{\circ}$K. Amorphous elemental metals crystallize at temperatures of tens of degrees K.

1.2.2 Amorphization By Solid-State Reaction (SSR)

The pioneering experiments in the synthesis of amorphous alloys by isothermal diffusion reactions were performed by Yeh et al.[1.10] They observed that upon charging the metastable crystalline alloy Zr_3Rh with hydrogen, it transformed into an amorphous hydride. This observation was explained in terms of a diagram of the free energy (Fig. 1.3) of the metastable and equilibrium phases involved, as a function of composition. When the metastable Zr_3Rh (Cu_3Au structure) reacts with hydrogen, the free energy of the system can be lowered via two alternative routes: an amorphous hydride $(Zr_3Rh)_{1-x}H_x$ can be formed or the alloy can phase-separate into a mixture of $Zr_{1-x}H_x$ and a Rh- rich crystalline phase. A coherent crystalline Zr_3Rh hydride is assumed to have a Gibbs free energy higher than the other phases involved, since it has never been observed. The phase separation into ZrH_2 + Rh or $Zr_{1-x}H_x$ + $(Zr_2Rh)_{1-y}H_y$ involves long-range interdiffusion of metal atoms, since interfacial energies between the phases require domains of a minimum size (≈20-30 Å). The time constant characteristic of a diffusion process is equal to

$$\tau = x^2/D \qquad (1.3)$$

where x is the diffusion length (minimum domain size) and D is the diffusion coefficient. Due to its small atomic size, the diffusion coefficient of a hydrogen atom in a metal lattice is orders of magnitude higher than self-diffusion of the metal atoms. Therefore, the time scale for the formation of an amorphous hydride is considerably

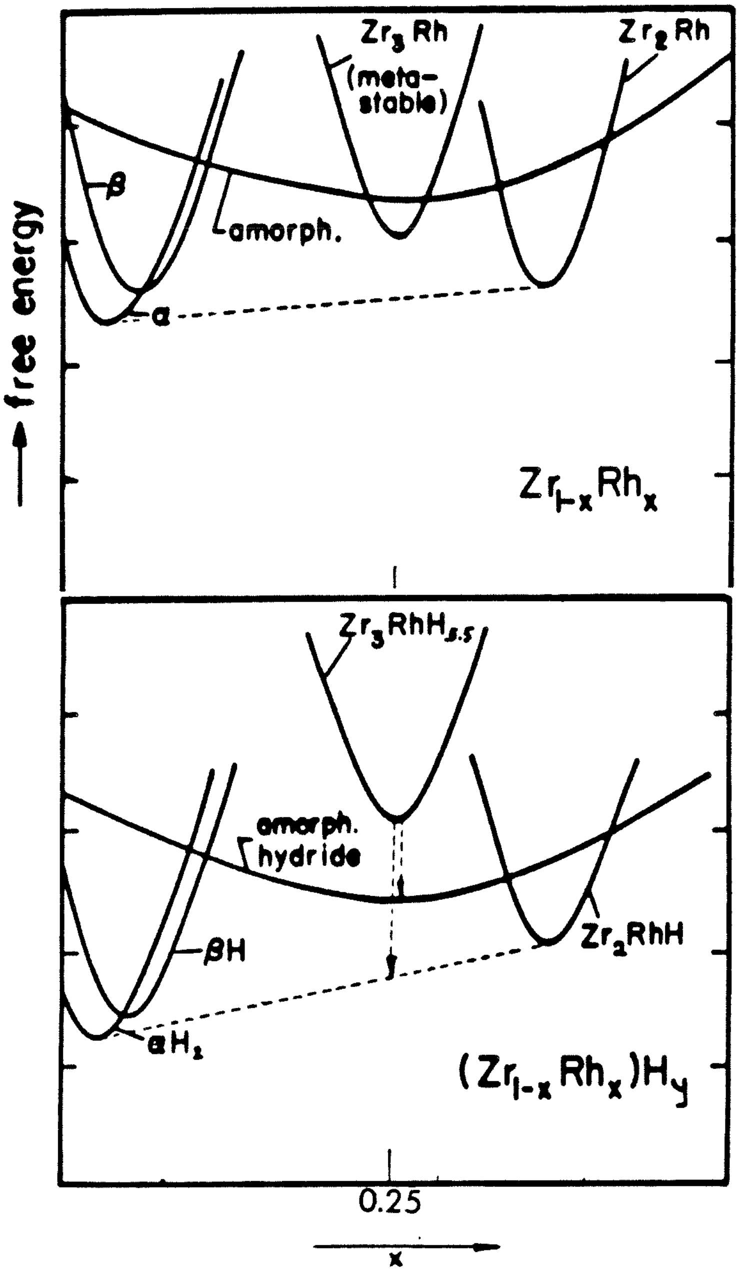

Figure 1.3 Hypothetical free energy diagrams for Zr_xRh_{1-x} and $Zr_xRh_{1-x}H_y$ (from Ref. 1.10).

smaller than that for phase-separation and the system becomes kinetically trapped in this metastable equilibrium.

The next important step in the study of amorphization by SSR was the demonstration of metal- metal reactions in thin films. Schwarz and Johnson[1.11] reacted multilayer thin films of elemental crystalline gold and lanthanum to form an amorphous Au-La alloy. Their samples consisted of alternating layers of the two metals, each several hundred angstroms thick. This configuration provided small diffusion distances together with a total thickness sufficient for performing X-ray diffraction experiments. In Fig. 1.4, X-ray diffraction patterns illustrate the reaction. As a result of thermal annealing, the intensity of the Bragg peaks originating in the elemental phases decreases, and a broad maximum grows, characteristic of an amorphous phase.

The metal-metal reaction can be understood on the basis of free-energy diagrams. In Fig. 1.5, the free energy of various phases in the binary Au-La system is plotted as a function of the composition. α and β denote the terminal solid solutions, and the dotted line represents the average free energy of a mixture of the pure crystalline elements. The free energy of the elemental crystalline phases was obtained from existing thermodynamic data, and that of the pure amorphous phases was extrapolated from the melting point:[1.12]

$$\Delta G_{x,l}(T) = (T_m-T)/T_m \; \Delta H_{x,l}(T_m) \qquad (1.4)$$

where $\Delta G_{x,l}(T)$ is the free-energy difference between the amorphous and crystalline phases, and $\Delta H_{x,l}(T)$ is the enthalpy of fusion. Having fixed the end points, the free energy of the amorphous phase was estimated

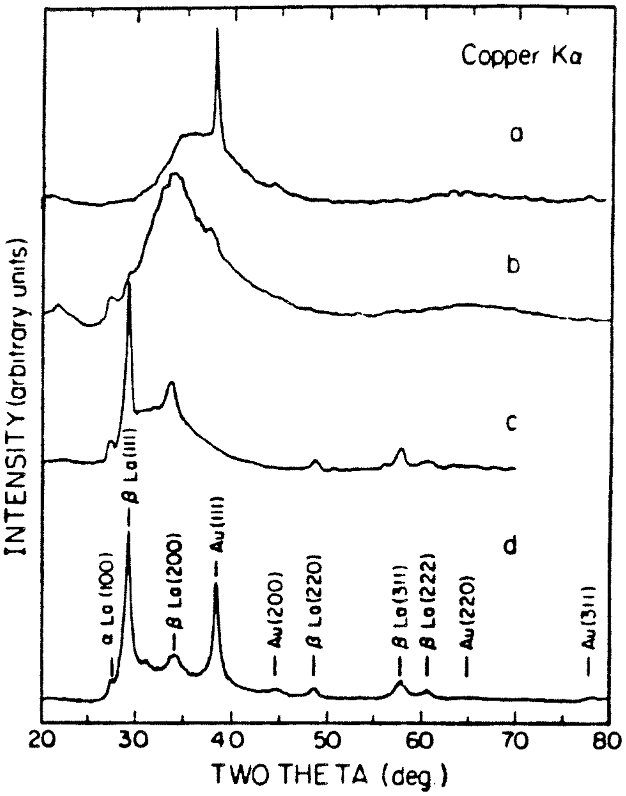

Figure 1.4 X-ray scattering intensity as a function of scattering angle for annealed (4 hr at 80 °C) samples of increasing La content (curves a, b and c) and for an unreacted sample with La content similar to that of curve b (from Ref. 1.11).

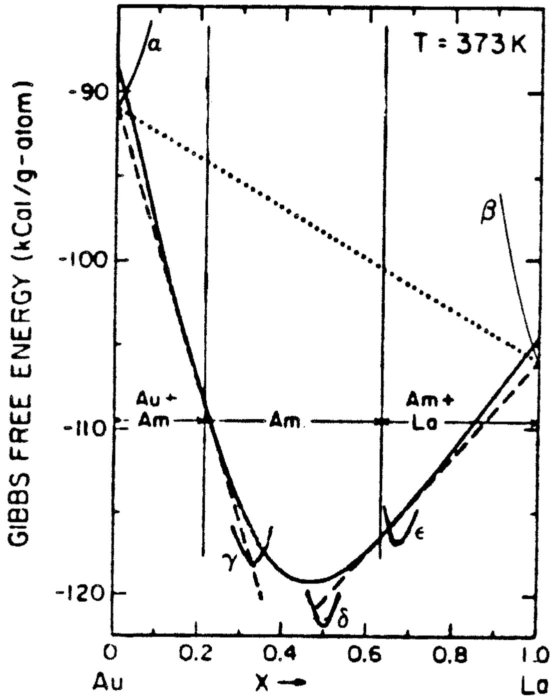

Figure 1.5 Gibbs free energy vs. composition for a mixture of crystalline Au and La (dotted line) and for amorphous Au_xLa_{1-x} alloy (from Ref. 1.11).

using Miedema's method[1.13] for the enthalpy of mixing and the entropy of a regular solution. The free energies of the intermetallic compounds lie below those of the amorphous phase and are indicated schematically. One can see that due to the large negative enthalpy of mixing of the elements, the initial elemental mixture can lower its free energy by mixing to form an amorphous phase. Crystallization would lower the free energy only by a small additional amount. If the diffusion reaction can proceed at sufficetly low temperature, so that the crystalline compounds cannot nucleate, an amorphous phase will result. In other words, there are two relevant time scales.[1.14] τ_x is the characteristic time for the nucleation of a crystalline phase and τ_a is the time it takes to complete the formation of an amorphous phase

$$\tau_a = L^2/D \tag{1.5}$$

where L is the layer thickness, assuming that amorphous phase formation is not nucleation-limited.[1.15] If $\tau_a << \tau_x$, amorphization can occur. Fig. 1.6 shows a schematic TTT diagram for the reaction. The solid line denotes the time required to transform a certain fraction into a crystalline compound. It is nose-shaped as in Fig. 1.2, because the driving force and the kinetics have an opposite temperature dependence. On the other hand, for the formation of the amorphous phase, the driving force remains roughly constant with temperature, while there is a rapid increase in the diffusion coefficient, so the curve is monotonic. Each type of transformation is described by a family of lines corresponding to different layer thicknesses. All experiments reported to date have been performed at isothermal conditions, below the "nose."

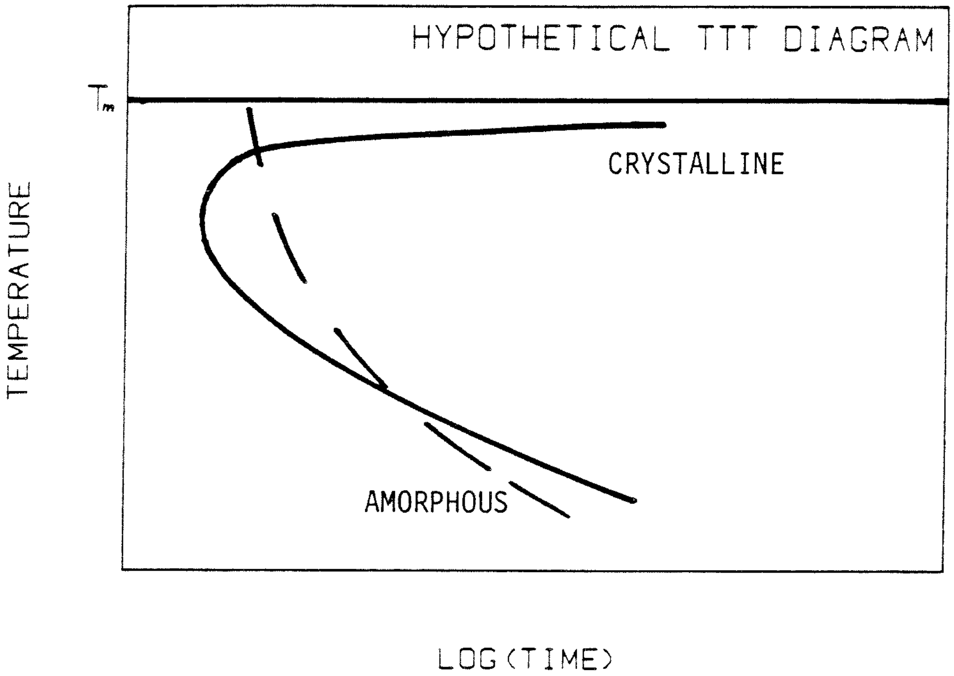

Figure 1.6 Hypothetical TTT diagram for a solid- state reaction of elemental phases. The solid line denotes a crystalline phase, the broken line the amorphous phase.

Solid- state synthesis of amorphous metal alloys has been studied for less than three years. Many questions are still open, and it is worthwhile reviewing the current state of understanding of the process. The systems reported so far are Zr- (Cu, Ni, Co)$^{1.16-1.18}$, La- (Au, Ag)$^{1.11,1.19}$, Y- Au$^{1.20}$, Er- (Ni, Cu)$^{1.21}$ and Hf-Ni.$^{1.15}$ They all satisfy the requirement of having a large negative heat of mixing. One can expect more systems to be reported in the future, and many early transition metal - late transition metal and rare earth - late transition metal pairs offer themselves as candidates.

It can be considered well established that the amorphous phase grows as a uniform layer. This has first been shown by means of Rutherford backscattering spectroscopy (RBS).$^{1.15}$ More recently, cross-sectional transmission electron micrographs of partially reacted thin film multilayers$^{1.22}$ showed actual real-space images of the reaction products, as reproduced in Fig. 1.7. The RBS spectra taken for samples reacted at different times and temperatures show that, for a fixed temperature, the thickness of the amorphous layer grows roughly as the square root of the reaction time, a behavior consistent with diffusion controlled growth.

An exothermic reaction between two elements is known to cause a reduction of the total volume due to a decrease in bond lengths. We would therefore expect to see Kirkendall voids$^{1.23}$ in reacted samples. This has indeed been observed in electron micrographs of Co-Zr$^{1.18}$ and Ni-Zr$^{1.24}$ multilayers.

It has been shown by Unruh et al.$^{1.25}$ that stresses have a strong effect on the reaction rates. They measured the rates for Ni-Zr sputtered multilayers by monitoring the intensity of the Bragg peaks of

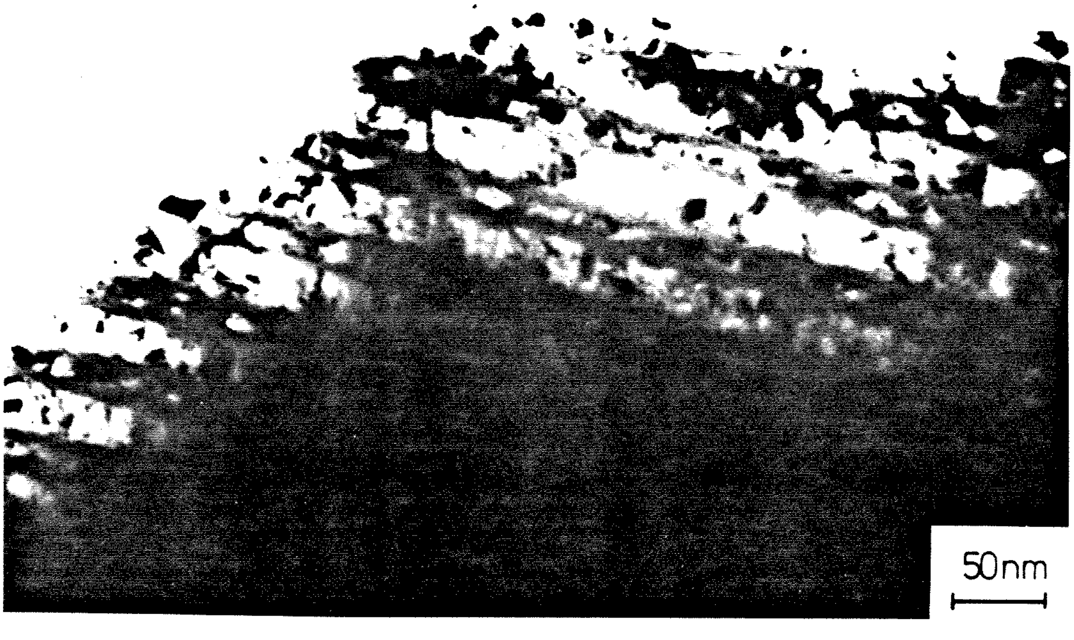

Figure 1.7 Cross- sectional transmission electron micrograph of partially reacted Co-Zr multilayers (from Ref. 1.22).

the elemental phases during isothermal anneals. The rate of decrease of the Bragg peaks, which is proportional to the rate of growth of the new phase, followed a $t^{1/2}$ law. The reaction was observed to occur at one rate for a certain time regime, and then go over to a lower rate, still obeying a $t^{1/2}$ law. This behavior could be correlated to a relief of initially high compressive stress, as monitored through the lattice constants.

1.2.3 The Structure of Amorphous Materials

In crystalline materials, there is long-range order which enables one to describe all atomic positions exactly (ignoring thermal motion). For amorphous materials, solid or liquid, one has to use information which is averaged over all atomic sites. A correlation function $\rho(|\vec{r}-\vec{r}_0|)$ can be defined, which denotes the average density of atoms at a distance $r=|\vec{r}-\vec{r}_0|$ from a specific atom at $\vec{r}_0$, averaged over all atomic positions $\vec{r}_0$ and spatial directions $\{\vec{r}\,|\quad |\vec{r}-\vec{r}_0|=r\}$. This gives a one-dimensional projection of the actual structure. Higher-order correlations have the form $\rho_n(\vec{r}_1, \vec{r}_2, \ldots, \vec{r}_n)$ = the probability of finding an atom at $\vec{r}_1$, given n-1 atoms at $\vec{r}_2, \ldots, \vec{r}_n$.

The correlation function $\rho(r)$ can be calculated from measured diffraction patterns (X-rays, neutrons or electrons). The general expression for the intensity scattered off a group of atoms is

$$I(\theta) = \sum_{n,m} f_m f_n \frac{\sin Kr_{mn}}{Kr_{mn}} \qquad (1.6)$$

where f_i is the form factor of the i^{th} atom, r_{mn} is the magnitude of the vector separating the n^{th} and the m^{th} atom, and K is the magnitude of the scattering vector $\vec{K}$ given by:

$$K = \frac{4\pi}{\lambda} \sin\theta \tag{1.7}$$

where θ is the scattering angle. The intensity depends on the scattering angle through K. For electron and X-ray diffraction, the form factors are K- dependent, unlike neutron scattering. For the sake of simplicity, we assume all form factors to be equal, and write separately the terms in the sum with m=n:

$$I(\theta) = Nf^2 \left(1 + \sum_{m'} \frac{\sin Kr_{mn}}{Kr_{mn}}\right) \tag{1.8}$$

where m' denotes that the summation excludes the atom at the origin. If we regard the distribution of atoms as a continuous function, we replace the sum by an integral

$$I = Nf^2 \left[1 + \int_0^\infty 4\pi r^2 \rho(r) \frac{\sin Kr}{Kr} dr\right] \tag{1.9}$$

$4\pi r^2 \rho(r)\, dr$ is the number of atoms contained in a spherical shell of thickness dr and radius r from the reference atom. Let ρ_0 be the average density of atoms; then

$$I = Nf^2 \left(1 + \int_0^\infty 4\pi r^2(\rho(r) - \rho_0) \frac{\sin Kr}{Kr} dr + \int_0^\infty 4\pi r^2 \rho_0 \frac{\sin Kr}{Kr} dr\right). \tag{1.10}$$

The last term is a delta function for a macroscopic homogeneous sample, i.e. the forward scattering. It is not seen in normal high-angle diffraction, and can be omitted. When there are density fluctuations in the scattering object, this term gives the small-angle scattering they produce. One obtains:

$$\frac{I_{obs.}}{Nf^2} - 1 = \int_0^\infty 4\pi r^2(\rho(r) - \rho_0)\,\frac{\sin Kr}{Kr}\,dr \quad . \qquad (1.11)$$

The transform can be inverted,

$$4\pi r(\rho(r) - \rho_0) = \frac{2}{\pi}\int_0^\infty K(I(K) - 1)\sin Kr\,dK \qquad (1.12)$$

where $I(K) = I_{obs.}(K)/(Nf^2)$. $G(r) = 4\pi r(\rho(r)-\rho_0)$ is called the reduced radial distribution function.

For specimens with more than one atomic species, one can define partial correlation functions as $\rho_{ij}(r)$ = the density of j- atoms at a distance r from a reference atom of type i. The observed scattering function is then a weighted average of the Fourier transform of the ρ_{ij}'s, an extension of equation 1.11. One can vary the weighting factors by using different wavelengths of radiation, or by substituting isotopes in neutron scattering.[1.26] For an n- component system, there are n(n+1)/2 independent partial correlation functions, and the same number of different measurements is needed in order to solve for them.

The usefulness of measured RDF's lies mainly in their comparison to those obtained from computer generated or other models. There have been attempts to model the structure of metallic glasses as microcrystalline, where crystal size effects, strains and other defects are the cause for the broadening of the Bragg peaks.[1.27] The agreement with experimental data was not satisfying. A more successful approach was the dense random packing of hard spheres (DRPHS).[1.28] It consisted of physically packing thousands of spheres and measuring their coordinates. Later models were generated by computer simulations, and soft potentials were introduced.[1.29] A further development was the introduction of two different sizes to simulate binary alloys.[1.30] The RDF's obtained from these models gave reasonable agreement with experiments. A comprehensive review of the subject is given by Cargill.[1.31]

1.3 DIFFUSION

Since the solid- state reactions described in the previous section involve atomic transport, a brief review of solid- state diffusion is given. It starts with the basic description of the diffusion of a dilute impurity in a matrix, based on linear response theory. The results are used to develop the theory of chemical diffusion, i.e., diffusion at large concentrations. The temperature dependence of the diffusion coefficient is discussed.

1.3.1 Impurity Diffusion

When atoms are placed in a non-uniform chemical potential, they move so that the system reduces its free energy. Using linear response theory,[1.32] we can express the flux of the ith species as follows:

$$j_i = - L_{ii} \frac{d\mu_i}{dx} \quad . \qquad (1.13)$$

The L_{ij}'s are called transport coefficients, and we neglect those with $i=j$. μ_i is the chemical potential of the ith species. We can use the activity coefficients defined by

$$\mu_i(c_i) = \mu_i^\circ + kT \ln(\gamma_i c_i) \tag{1.14}$$

where μ_i° is the chemical potential of the i^{th} species when it is a pure phase and c_i is its concentration. We obtain

$$j_i = - L_{ii} kT \frac{d\ell n\, \gamma_i c_i}{dx} = - L_{ii} \frac{kT}{c_i} \left(1 + \frac{d\ell n \gamma_i}{d\ell n c_i}\right) \frac{dc_i}{dx} \quad . \tag{1.15}$$

$(1+ \frac{d\ln\gamma_i}{d\ln c_i})$ is called the chemical factor, and it is equal to one for ideal solutions. For a regular solution in the dilute limit, γ_i becomes independent of the concentration and the equation reduces to

$$j_i = - D_i \frac{dc_i}{dx} \tag{1.16}$$

where

$$D_i = L_{ii}\, kT/c_i \tag{1.17}$$

is the impurity diffusion coefficient for the component i.

1.3.2 Diffusion at High Concentrations

Suppose one component in a diffusion couple moves considerably faster than the other- $D_1 >> D_2$. As a result, there is a net motion of the lattice planes in the laboratory coordinate system. One observes a net flux of material in the direction in which the faster component is moving- the Kirkendall effect. To express the net fluxes in the lattice frame of reference, one needs to subtract the net lattice motion. Assume that the transport coefficients are the same as in the dilute limit; one then obtains:

$$j_1 = - \frac{c_1 D_1}{kT} \frac{d\mu_1}{dx} - v_1 c_1 \qquad (1.18a)$$

$$j_2 = - \frac{c_2 D_2}{kT} \frac{d\mu_2}{dX} - v_2 c_2 \qquad (1.18b)$$

where v_L is the lattice velocity. By definition

$$j_1 + j_2 = 0 \qquad (1.19)$$

and since the system is in equilibrium, the Gibbs- Duhen relationship holds

$$c_1 d\mu_1 + c_2 d\mu_2 = 0. \qquad (1.20)$$

One obtains for the net lattice velocity:

$$v_L = (D_2 - D_1) \frac{N_1}{kT} \frac{d\mu_1}{dx} \qquad (1.21)$$

where N_1 is the mole fraction of type 1 atoms,

$$N_1 = c_1 V_m \tag{1.22}$$

and V_m is the molar volume. Substitution into equ. 1.18 gives

$$j_1 = - j_2 = - (N_2D_1 + N_1D_2) \left(1 + \frac{d\ell n\gamma_1}{d\ell nc_1}\right) \frac{dc}{dx} \quad . \tag{1.23}$$

This equation was first derived by Darken[1.33]. If one uses the entropy of mixing of an ideal solution:

$$\Delta S = -k(N_1 \ln N_1 + N_2 \ln N_2) \tag{1.24}$$

and an enthalpy of mixing of the form:

$$\Delta H_{mix} = \alpha N_1 N_2 \tag{1.25}$$

and notes that the chemical potential of a species is the derivative of the Gibbs free energy with respect to the atomic density:

$$\mu_i = \frac{dg}{dc_i} \quad , \tag{1.26}$$

one then obtains

$$\left(1 + \frac{d\ell n\gamma_1}{d\ell nc_1}\right) = \left(1 - \frac{2\Delta H_{mix}}{kT}\right) \quad . \tag{1.27}$$

A negative heat of mixing enhances diffusion and a positive heat of mixing inhibits it. Moreover, if the heat of mixing is positive and sufficiently high, the diffusion coefficient becomes negative and atoms diffuse up the concentration gradient. This is the case of spinodal decomposition.[1.34]

1.3.3 Thermal Activation

The microscopic theory of diffusion will not be addressed in detail, and we shall only look at the principles of the temperature dependence of the diffusion coefficient.[1.35] Let us calculate the rate of jumps of an interstitial atom in a solid. The potential of every site will be approximated as harmonic. The probability that it occupies a state with the energy

$$E_i = h\omega \left(i + \frac{1}{2}\right) , \tag{1.28}$$

will be

$$p(E_i) = \frac{e^{-E_i/kT}}{\sum_i e^{-E_i/kT}} . \tag{1.29}$$

The atom will jump to a neighboring site if its energy exceeds the barrier height ω_0. The probability for it is

$$p(E > \varepsilon_0) = \frac{\sum_{E_i > \varepsilon_0} e^{-E_i/kT}}{\sum_i e^{-E_i/kT}} . \tag{1.30}$$

For $\hbar\omega << kT$ one can approximate the sum by an integral

$$p(E > \varepsilon_0) = \frac{\int_{\varepsilon_0}^{\infty} e^{-E/kT}\, dE}{\int_0^{\infty} e^{-E/kT}\, dE} = e^{-\varepsilon_0/kT} \quad . \tag{1.31}$$

The rate at which the atom jumps to a neighboring site can then be expressed as

$$\omega = \omega_0 \, e^{-\varepsilon_0/kT} \tag{1.32}$$

where ω_0 is the frequency at which the barrier is approached. Since the diffusion coefficient is proportional to the jump frequency and to the square of the jump distance and the latter is approximately independent of temperature, we can write

$$D = D_0 \, e^{-\varepsilon_0/kT} \quad . \tag{1.33}$$

Other diffusion mechanisms can be treated in a similar fashion. The activation energy ε_0 then has a different meaning, e.g., for vacancy jumps it is the energy required for an atom to jump into a vacant site. If one mechanism is dominant at a certain temperature, then one can obtain the activation energy from the slope of the lnD vs. 1/T plot, called the Arrhenius plot.

1.4 *IN SITU* COMPOSITES

Composite materials, i.e., materials consisting of more than one phase, have been the subject of many studies. In particular, ultrafine metallic composites have been studied for over 20 years[1.36] for their mechanical, thermal and electrical properties. They exhibit unusual behavior due to their high density of interfaces. Sacharoff et al.[1.37] were able to form composites containing platinum wires 200 Å in diameter and to observe one- dimensional effects.

There are two major methods of preparing *in situ* composites: rapid solidification and mechanical deformation.[1.38] The first is based on rapidly solidifying a liquid alloy of elements which are immiscible in the solid state. The size of the lamellae or filaments obtained can be controlled by varying the cooling rate. A related method is the decomposition of a homogeneous alloy in the solid state. The above technique requires a positive heat of mixing of the constituent elements and is therefore inherently inapplicable for the amorphization by solid-state reaction, where a large negative heat of mixing is the required driving force. The second method consists of physically mixing the constituent elements (in form of powders or foils) and then mechanically deforming them. The mechanical deformation creates dislocations, and their density was observed to be as high as 10^{12}- 10^{13} per cm^2.[1.39] However, for high deformation ratios, when the filament sizes decrease below several hundred Å, the dislocation density decreases dramatically. Frommeyer and Wassermann[1.40] suggest that the interfaces act as sinks for dislocations. A review of *in situ* composites was given by Bevk.[1.38]

2. EXPERIMENTAL TECHNIQUES

2.1 SAMPLE PREPARATION

2.1.1 *In situ* Composites[1.1]

The instrument used for mechanical deformation was the rolling mill (Fig. 2.1). It consists of two parallel steel rollers which rotate in opposite directions, the spacing between them being continuously adjustable. A metal sample put between them is pulled by frictional forces and its thickness is reduced by plastic deformation, due to the applied compressive stress. The deformation process is done in small successive steps, to avoid heating and damage due to excessive stress.

The elemental materials used for preparing the physical mixtures were in foil or powder form. The purity of the materials used is listed in Table 1. The powder method was used only for Ni-Zr, with an average grain size of 40 μm for both metals. The zirconium powder was received in an argon atmosphere and was handled in argon gas until after compaction. After determining the composition by weighing the powders (in a glove box), they were mixed and tumbled for 24 hours. The mixture was compacted in a die under a pressure of 4 GPa to form an ingot of 1/2" diameter. The ingot was then sealed in a stainless steel capsule under high vacuum, using electron beam welding. The container with the sample was flat-rolled in a rolling mill, reducing the sample thickness by a factor of 8, and the resulting foil was removed from the stainless steel. Then the sample was deformed in 10-12 passes, each consisting of: 1) folding the foil to double its thickness, 2) rolling it between two 0.75 mm thick stainless steel plates to the smallest spacing of the

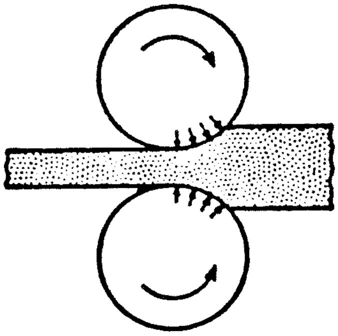

Figure 2.1 Schematic diagram illustrating a rolling mill (from Ref. 2.2).

	FOILS				POWDERS	
Metal	Zr	Er	Cu	Ni	Zr	Ni
Metal Purity	4N	3N	5N+	4N8	3N	3N
Total Purity		<0.1 at. % H_2	5N		2N7	

Table 2.1 Purity of metal foils and powders used for composites.

rollers. The foils were prepared by rolling commercially available foils or pieces to a thickness of 10-20 μm. The sample composition was controlled by varying the relative thickness of the constituent foils, and an accurate determination was made by weighing them. To minimize oxidation effects, all steps were done without interruption after the foils had been prepared. The two elemental foils were first brought into contact and wound to form a spiral (Fig. 2.2). The spiral was rolled inside a stainless steel tube to the limit of the rolling- mill and the resulting foil removed. Subsequently, the same process was used as that employed for the foil resulting from powder. The number of passes was as high as 55 for the erbium alloys. Both methods produced somewhat brittle foils. The final thickness of foils of the erbium-based alloys reached 200 μm, and it could be increased as desired by stacking several plates and bonding them through mechanical deformation.

An important parameter for the sample preparation process is its temperature rise during the rolling. Erbium-based composites reacted at annealing temperatures as low as 70 ^{o}C, so heating effects during rolling had to be considered. For these samples, the transient temperature was monitored by sandwiching a chromel- alumel thermocouple between two sample foils while these were being deformed between stainless steel plates (see Fig. 2.3). (Several tenths of a second after deformation, the thermocouple was broken as it was pulled by the rolling mill.) The voltage signal was monitored with a storage oscilloscope with a time resolution of less than one msec. The thermocouple wire was insulated with Teflon sleeves while leaving an exposed section smaller than the sample size.

To obtain a high purity environment for annealing the samples, the

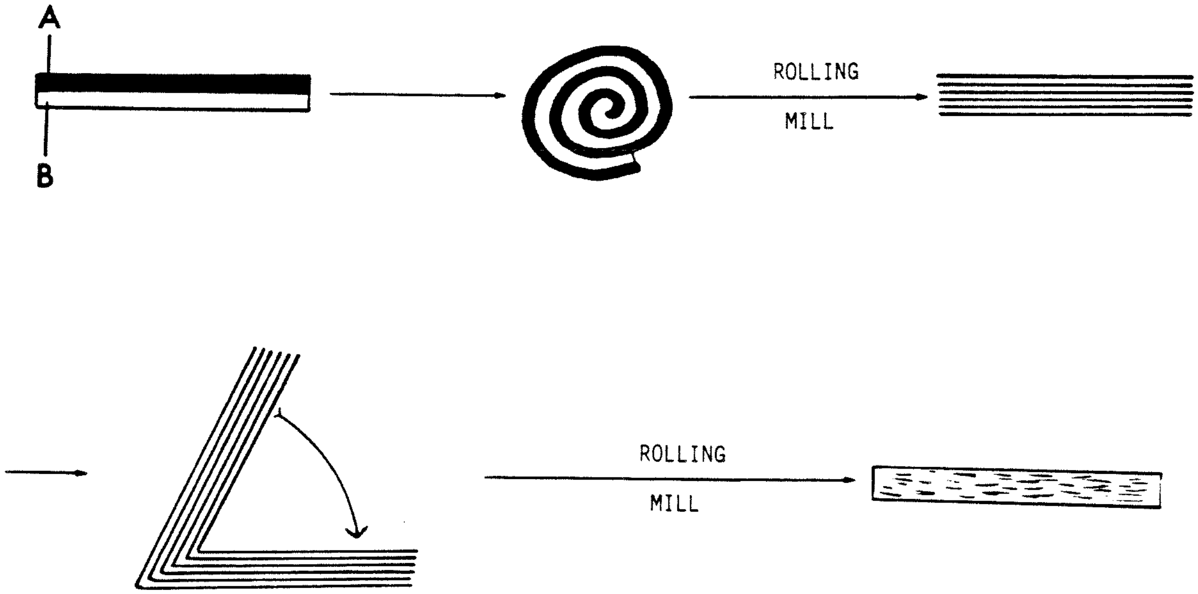

Figure 2.2 Preparation of a composite from elemental foils.

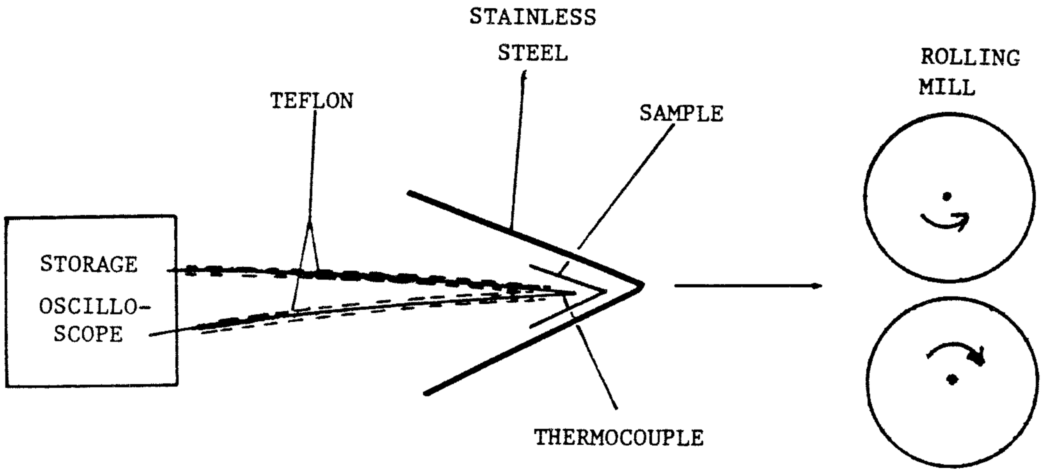

Figure 2.3 Measurement of transient temperature during sample deformation.

following procedure was applied: the samples were vacuum-sealed in long Pyrex ampules together with zirconium foils. The zirconium was heated to 550 °C for 10 hours while the sample was kept at ambient temperature at the opposite end of the ampule. The high reactivity of zirconium makes it useful as a getter for gas impurities such as oxygen, water and hydrocarbons. After cooling the ampule, the sample was moved to the other side of the ampule and annealed. Samples annealed on the side which had been cold during the gettering process showed signs of contamination. This was due to the lesser amount of outgassing of the walls on the cold side of the ampule.

2.1.2 Film Deposition

Thin films were deposited on Pyrex substrates by thermal evaporation from tungsten boats. The boats were heated by electric currents of 5- 15 Amperes. A shutter above the boats had a magnet attached to it and could be moved with a magnet external to the system during deposition. Its control enabled deposition from one source at a time or co-deposition from two sources to produce an amorphous alloy. Prior to evaporation, the substrates were cleaned in an ultrasonic cleaner with a detergent and then with high purity ethanol. The pumping system consisted of a mechanical pump (for pumping down to $\simeq 10^{-2}$ torr) and of a diffusion pump backed by a mechanical pump and assisted by a liquid nitrogen cold trap. After baking out the system by heating the tungsten boats to moderate temperatures without melting the sources, the vacuum reached the 10^{-7} torr range. During deposition, it increased to the 10^{-6} torr range. The metal films were deposited at typical rates of 10-30 Å/sec. The substrate temperature was controlled with Peltier heaters placed between the substrates and a water- cooled copper plate (Fig. 2.4). Depending on the direction of the current in the Peltier junctions, the samples could be either heated or cooled. The substrates were heated before deposition in order to bake them out, and after deposition to anneal the samples. During deposition, the substrates were cooled to avoid heating of the films by radiative heat transfer from the sources. There were four substrates in the system, with pairs placed symmetrically with respect to the sources, so as to give the same film composition on the two members of each pair. After deposition, one film from each pair was kept at 0 °C while the other was being annealed. This method made possible the comparison of two almost identical films, one unannealed and the other annealed *in situ* , i.e., without being exposed to the atmosphere after deposition.

The thickness of the evaporated films was monitored with a Dektak thickness monitor, which scans the film surface with a stylus and monitors the stylus position. Since some areas at the edges of the films are shielded from one source by shadow effects, one could measure separately the amount of material deposited from each source. Assuming the densities of the elemental films had the same values as the bulk, one could use these results to estimate the compositions of the alloy films. For samples measured with Rutherford backscattering, a more accurate determination of the composition was made.

2.1.3 Rapid Cooling from the Melt

The synthesis of metallic glasses by rapid cooling from the melt is based on heat transfer from a thin layer of sample material to a bulk heat sink, which is a good thermal conductor (usually copper).

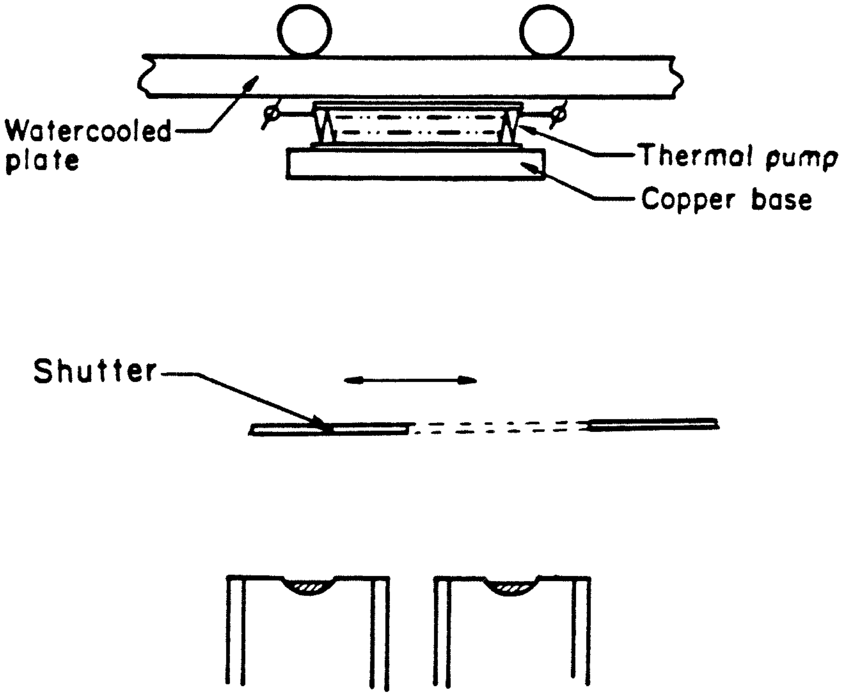

Figure 2.4 Arrangement of Peltier heaters/ coolers in vacuum deposition system (from Ref. 2.3).

In the "gun" method[2.4] (Fig. 1.1b), the liquid alloy is atomized by a shock wave created by high gas pressure breaking a Mylar diaphragm. The metal droplets hit a copper substrate, thereby overlapping and form a foil of non-uniform thickness (10^{-6} to 10^{-3} cm). The cooling rate for this method is ~10^7 deg/sec . Some regions of the foils produced by this method are thin enough to be observed in a transmission electron microscope.

In melt-spinning (Fig. 1.1a), one injects the molten alloy onto a spinning copper wheel, while its surface moves at a linear speed of about 40 m/sec. The metal is molten by induction heating through an rf coil, and the process takes place in an evacuated chamber. A ribbon of 10-30µm thickness and one or more mm width is obtained. Some similar industrial processes can produce wide sheets. The cooling rate for melt-spinning has been measured to be approximately 10^6 deg/sec.

The "piston and anvil" (Fig. 1.1b) is an apparatus in which a liquid drop is released and falls between two flat copper heads. When the drop passes between a light source and a photodetector placed above the heads, one of them (the piston) is accelerated by high gas pressure after a certain (adjustable) delay and the drop is smashed between the piston and the anvil. As a result, a foil of ≅50 µm thickness and 2-3 cm diameter is obtained. The process takes place in an inert gas atmosphere. Here the foil is cooled on both sides, so, despite the larger thickness, the cooling rate is about the same as for melt-spinning. The foils produced by this method are convenient for X-ray diffraction, where large and flat samples are needed.

2.2 X-RAY DIFFRACTION

The geometry used for X-ray diffraction experiments was $\Theta - 2\Theta$ (Fig. 2.5); i.e., the detector rotates at twice the rate of the sample. All samples were used in reflection geometry, unless the texture analysis required the scattering vector $\vec{K}$ to be in the plane of the sample. The reflection geometry allows the use of a wide (1°) divergent slit to obtain high intensities, since the sample focuses the beam and the angular resolution does not suffer (Fig. 2.6). The magnitude K of the scattering vector is given by

$$K= \frac{4\pi}{\lambda} \sin\Theta \quad . \tag{2.1}$$

For the qualitative scans, the K_α radiation of a copper target was used, which has wavelength $\lambda = 1.54$ Å. The K_β line was eliminated by using a nickel filter. For measuring the radial distribution functions, higher K values (up to 15 Å^{-1}) were accessed by using Mo K_α radiation (wavelength 0.7107 Å). The quantitative analysis required a monochromatic radiation, and a LiF crystal was used as a monochromator. It was placed in an orientation such that only the Bragg reflection of the Mo K_α line reached the detector (Fig. 2.7). The sample covered the area illuminated by the beam and its thickness was at least three times the absorption depth for the radiation used. This insured the practical elimination of substrate contributions to the signal and made the use of the infinite thickness approximation possible. For amorphous materials, the angular resolution did not need to be high, and 0.5° receiving slits were used in order to obtain high intensity.

The interference function measured was normalized by fitting its high K part to the weighted form factors given by Chromer et al.[2.7-2.10]

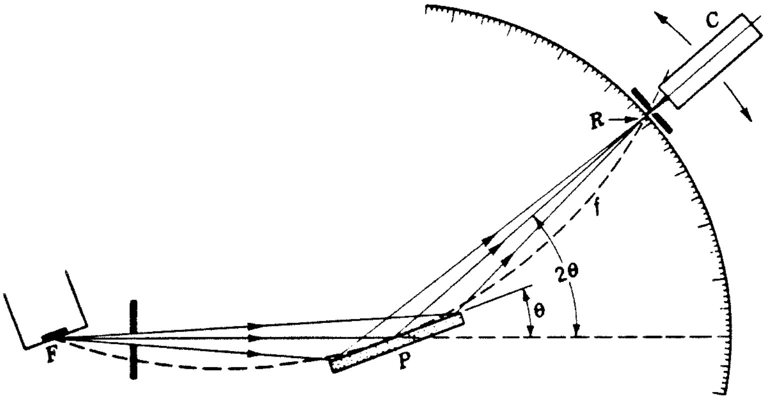

Figure 2.5 X-ray diffractometer in Θ - 2Θ geometry (from Ref. 2.5). F- source, P- sample, R- receiving slit, C- detector.

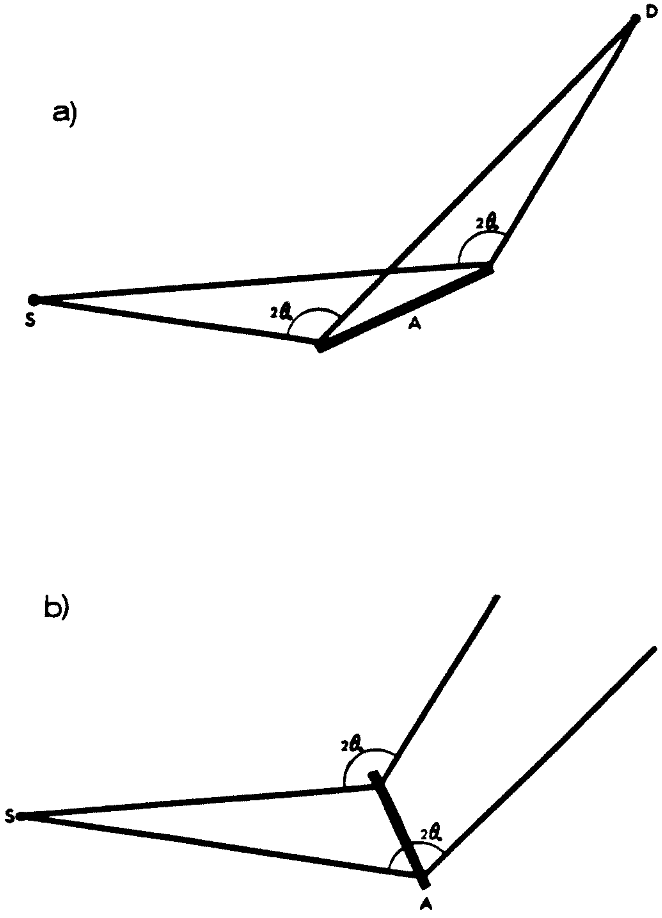

Figure 2.6 X- ray diffraction in reflection (a) vs. transmission (b) geometry.

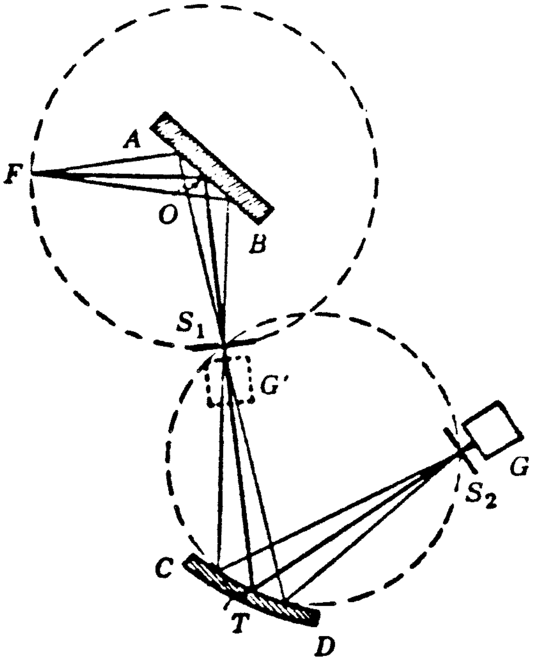

Figure 2.7 Use of crystal monochromator with diffractometer (from Ref. 2.6). A- sample, F- source, S_1- receiving slit, monochromator, S_2- detector slit, G- detector.

For details of the data analysis, see Williams.[2.11]

2.3 DIFFERENTIAL SCANNING CALORIMETRY (DSC)[2.12]

DSC is a method of measuring the heat capacity of materials between liquid nitrogen temperature and several hundred degrees centigrade. Phase transformations in materials involve the release or absorption of heat, i.e., a singularity in the heat capacity, for first-order transitions, or a discontinuous change in the heat capacity for second-order transitions. Therefore, the DSC is a very sensitive probe for monitoring such transformations. The DSC is based on the following principle (Fig. 2.8c): Two metal pans are placed symmetrically in a cell; one of them contains the sample (typically ≈10 mg) and the other serves as a reference. Each is heated with a separate heating element and the power input for each is controlled to give the same temperature and a constant heating rate. One records the difference in input power between sample and reference as a function of temperature. The signal is then proportional to the heat capacity,

$$dH/dT = mC_p dT/dt \qquad (2.2)$$

where dH/dt is the power put into the sample, m is its mass, C_p is the heat capacity at constant pressure and dT/dt is the heating rate.

The above procedure is employed in instruments built by the Perkin Elmer and Mettler companies. The DuPont DSC is based on a simpler principle (Fig. 2.8b). Only one heat source is used, and the temperature difference between sample and reference is used to evaluate the difference in heat fluxes. In using this method one neglects the

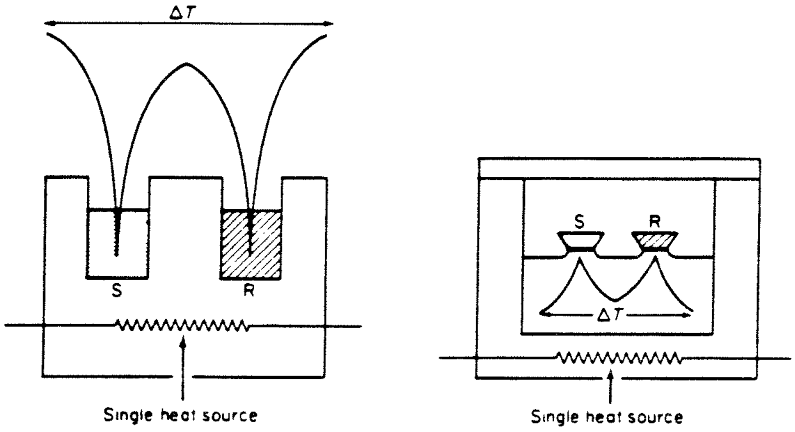

(a) Classical DTA

(b)'Boersma'DTA

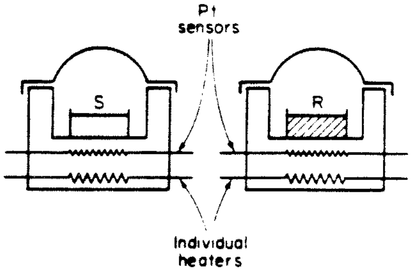

(c) DSC

Figure 2.8 Schematic representation of the three principal thermal analysis systems (from Ref. 2.12).

variation in the heat capacity which arises because the sample temperature varies slightly from the program temperature. In fact, this variation can become large at points at which there is a strong exothermic or endothermic transformation.

The DSC is a very delicate instrument. The cell has to be highly symmetrical, so that the two positions (sample and reference) receive the same heat flux (in the absence of a sample) and experience the same loss of heat to the environment. Even minute amounts of contaminants change the measured signal, since they introduce asymmetry into the cell, and may react with the sample.

Most experiments reported in this thesis were performed on the DuPont DSC 1090 at the Jet Propulsion Laboratory. The baseline was measured by running the instrument with two empty pans at the same heating rate as in the actual measurement. It was subtracted from the measured signal.

3. SOLID-STATE REACTIONS IN BULK COMPOSITES

3.1 INTRODUCTION

The motivation of the work presented in this chapter was the extension of the diffusion couple experiment on solid- state reaction to three dimensions. In addition to making possible the synthesis of amorphous alloys in bulk form for various applications, these experiments made feasible the application of new characterization techniques to the amorphous products of SSR.

Early attempts to achieve SSR in powder compacts of nickel and zirconium were not successful. One reason may be the fact that the grain sizes (above 1 μm) were larger than the layer thicknesses in previous thin film experiments- typically 500 Å. This makes diffusion distances large and the ratio of interfacial area to volume small, thereby reducing the reaction rate. A second and major reason for not being able to observe a potential reaction is the presence of surface contaminants on the powder grains acting as diffusion barriers. Such contaminants are present on powder surfaces in all practical cases even when the powders are handled carefully. The mechanical deformation of the powder compacts solves both of the above problems. In addition to consolidating the compact, it increases the interfacial area, thus creating intimate metal- metal interfaces. It also reduces the thickness of the layers, making diffusion possible in practical time spans.

The first systems selected for this study were Ni-Zr and Cu-Zr. All three elements are ductile and can be mechanically deformed without extensive embrittlement. Ni-Zr was selected because it was reported to produce amorphous phases in thin-film reactions.[3.1] The Cu-Zr system was chosen because of its similarity to Ni-Zr and the extent of available data for the corresponding rapidly quenched alloys to which our results could be compared. The heats of mixing calculated by Niessen et al.[3.2] are -49 kJ/mol for liquid NiZr and -23 kJ/mol for liquid CuZr. Direct calorimetric measurements for the Cu-Zr system reported by Kleppa and Watanabe[3.3] show somewhat smaller absolute values. Their data for the heat of mixing of liquid Cu and Zr are shown in Fig. 3.1. Zirconium-based composites embrittled after 12 passes of deformation, limiting the extent to which the layers could be reduced. Therefore, erbium- based composites were chosen for a subsequent series of experiments. Erbium is extremely ductile and does not work-harden under extreme deformation. It is one of the few rare-earth elements which are relatively inert in air. In addition, there is much interest in rare earth alloys of the rare-earth - late transition-metal type for magnetic applications. One can estimate the heat of mixing for the Er-Cu system based on Ref. 3.4, which gives calorimetric data for dilute solutions of erbium in liquid copper. If we use the heat of mixing of a regular solution as a first approximation, we obtain a heat of mixing of -23 kJ/mol for ErCu. We are not aware of any data concerning the enthalpies of mixing for the Ni-Er system. However, Miedema[3.5] has reported a general proportionality between negative heats of mixing and the number of intermetallic compounds in binary systems. Therefore, based on the existence of a number of crystalline intermetallic compounds in the Ni-Er system, we assume the heat of mixing to be negative and large.

3.2 SSR IN ZIRCONIUM-BASED COMPOSITES

Ni-Zr composites were prepared by the powder- metallurgical method

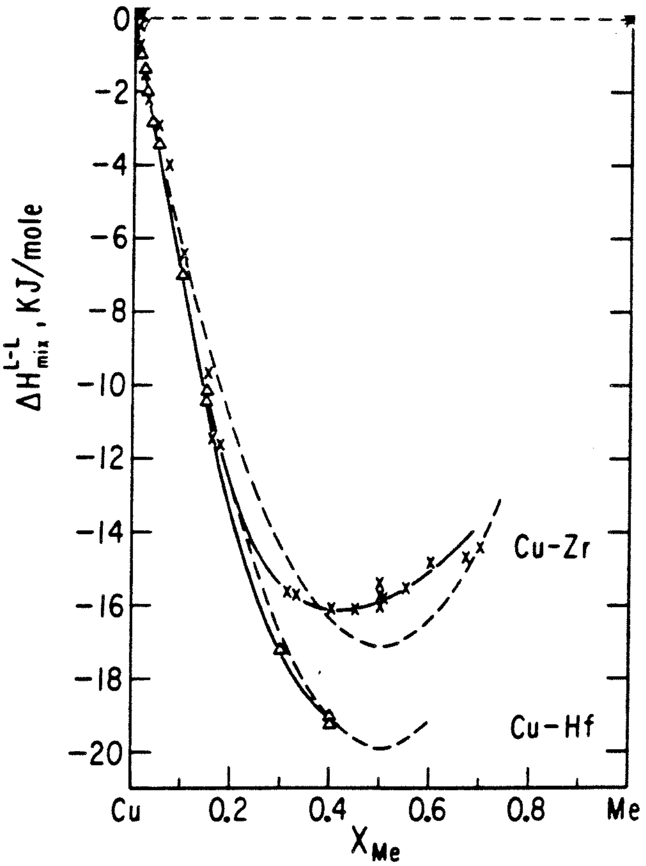

Figure 3.1 Enthalpy of liquid-liquid mixing for copper-zirconium (from Ref. 3.3). The broken line denotes a regular solution fit.

and both Ni-Zr and Cu-Zr composites were prepared from elemental foils. Most samples were prepared in 12 passes; i.e., the nominal reduction ratio was 2^{12} ($\cong$ 4000). This was the maximum attainable number of passes before the sample began to disintegrate due to embrittlement. A scanning electron micrograph taken of a cross section of a Ni-Zr sample prepared by the powder metallurgical technique is shown in Fig. 3.2. A layered morphology is observed with layer thicknesses on the order of 1000 Å.

Since the penetration depth of Cu K_α radiation in the above elements is 10- 20 μm, a diffraction experiment shows the contribution of many layers. Figs 3.3a and 3.4a show the diffraction patterns for as rolled $Ni_{62}Zr_{38}$ and $Cu_{60}Zr_{40}$. In both composites, strong texture is observed. The Ni (220) peak is unusually strong, in agreement with textures reported for cold-worked FCC metals.[3.6] Among the Bragg peaks corresponding to zirconium, the (100) is barely present and the (002) is relatively intense. Fig. 3.5a illustrates the texture by showing diffraction patterns of the same samples as those depicted in Fig. 3.3a, but taken in transmission geometry. Such diffraction geometry shows only lattice planes whose normals are parallel to the foil surface, whereas reflection shows only lattice planes whose normals are perpendicular to it.

According to Friedel,[3.7] strain fields produce broadening of the Bragg peaks ΔK given by

$$\Delta K = A\langle e^2\rangle^{1/2} K \tag{3.1}$$

where $\langle e^2\rangle^{1/2}$ is the rms strain. A is a geometrical constant approximately equal to one for a random distribution of dislocations. In

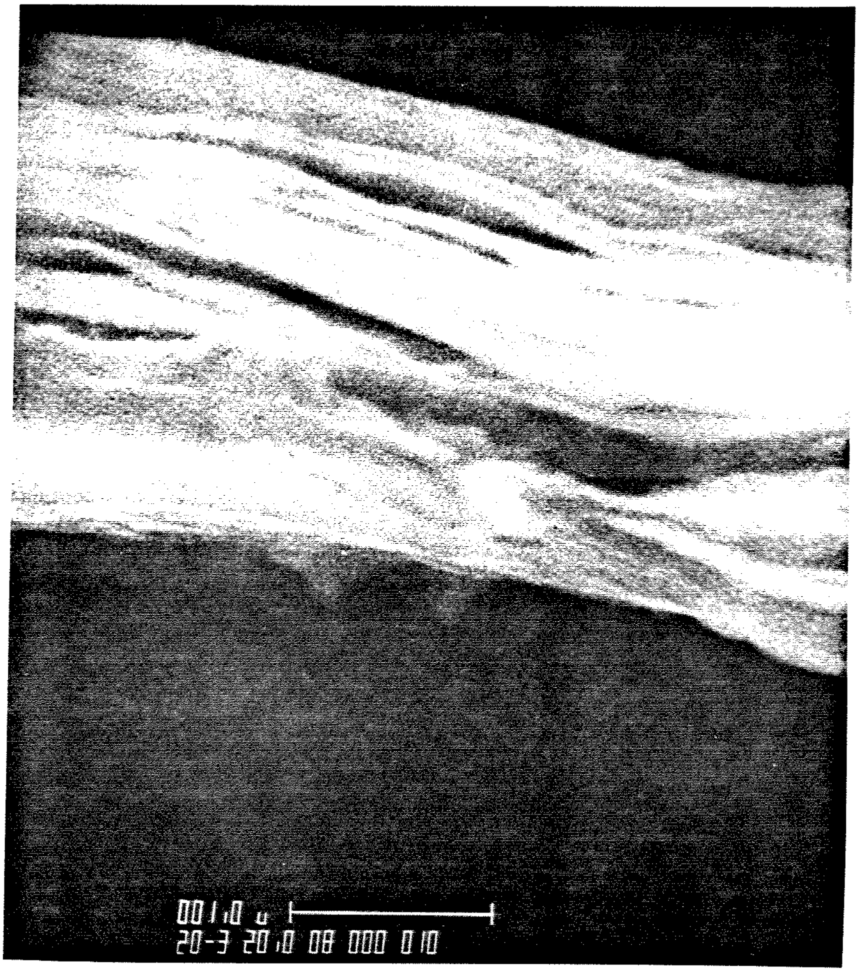

Figure 3.2 Scanning electron micrograph of a cross section of a Ni-Zr composite foil, as rolled.

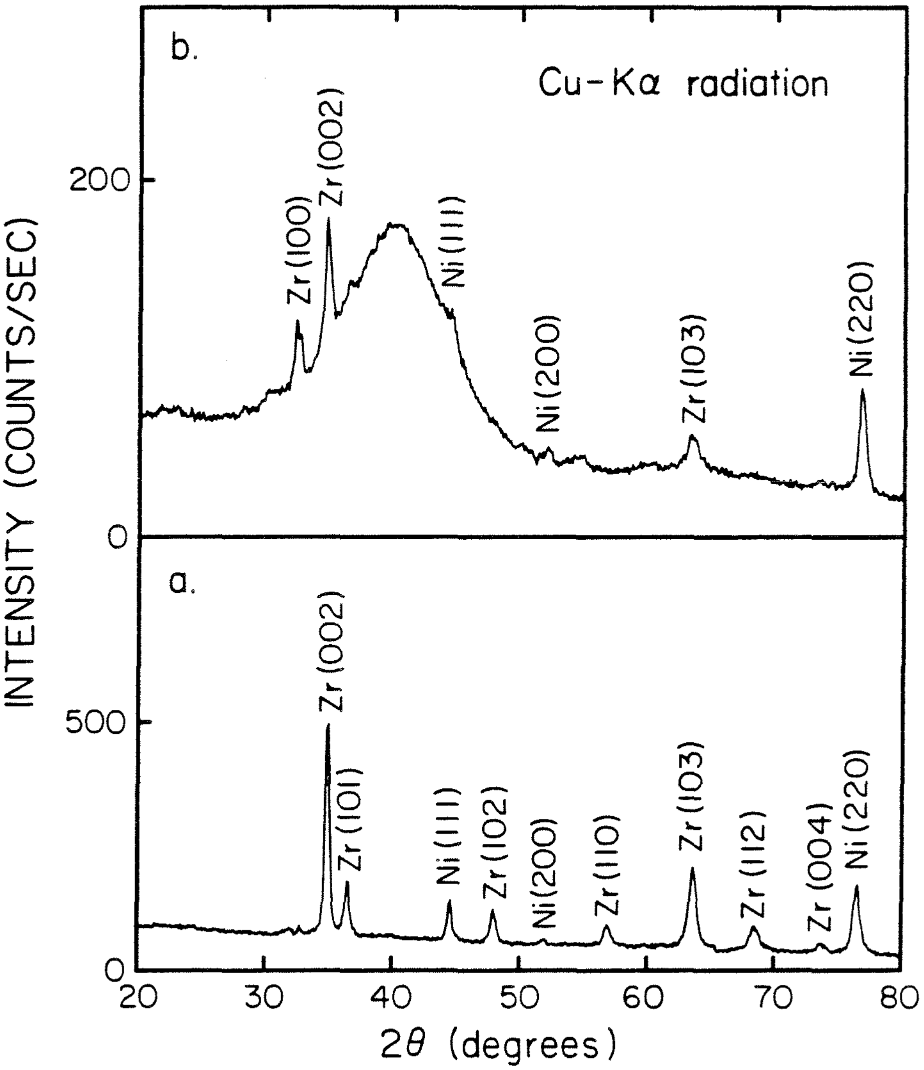

Figure 3.3 X-ray scattering intensity as a function of scattering angle for a $Ni_{62}Zr_{38}$ composite (a) as rolled and (b) reacted at 260 °C for 14 hr.

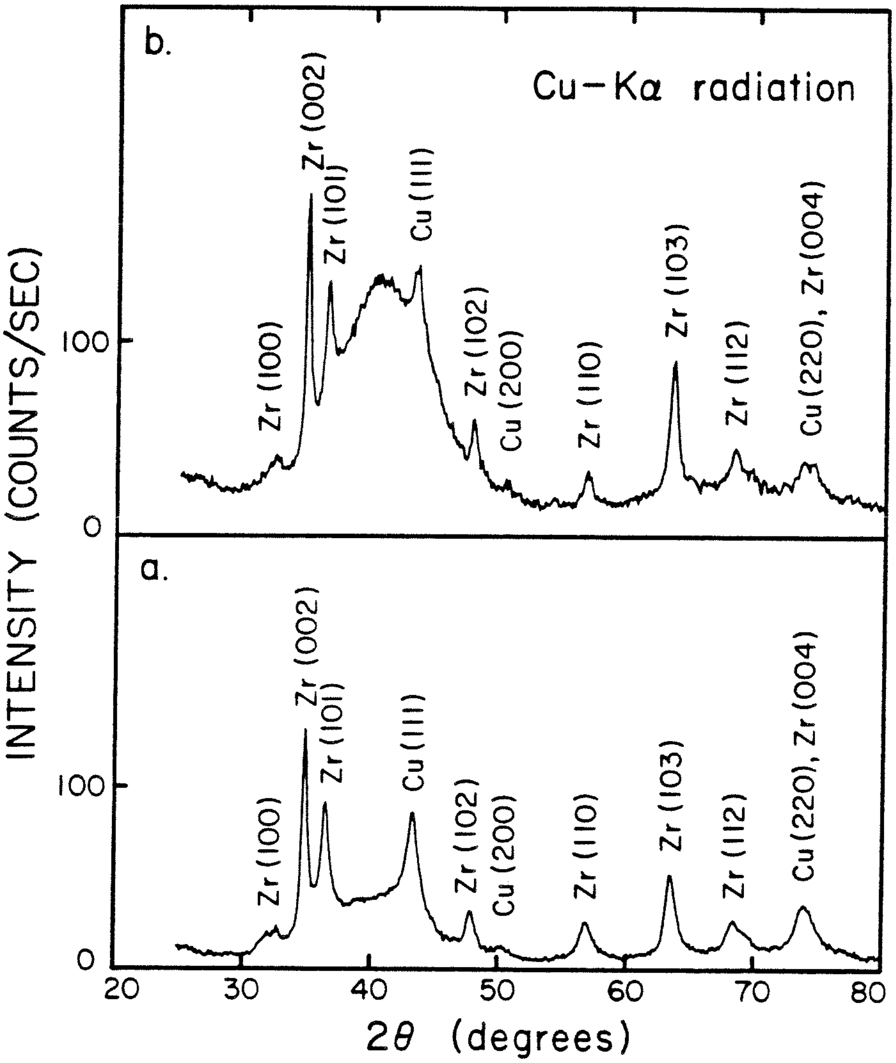

Figure 3.4 X-ray scattering intensity as a function of scattering angle for a $Cu_{60}Zr_{40}$ composite (a) as rolled and (b) reacted at 275 °C for 8 hr.

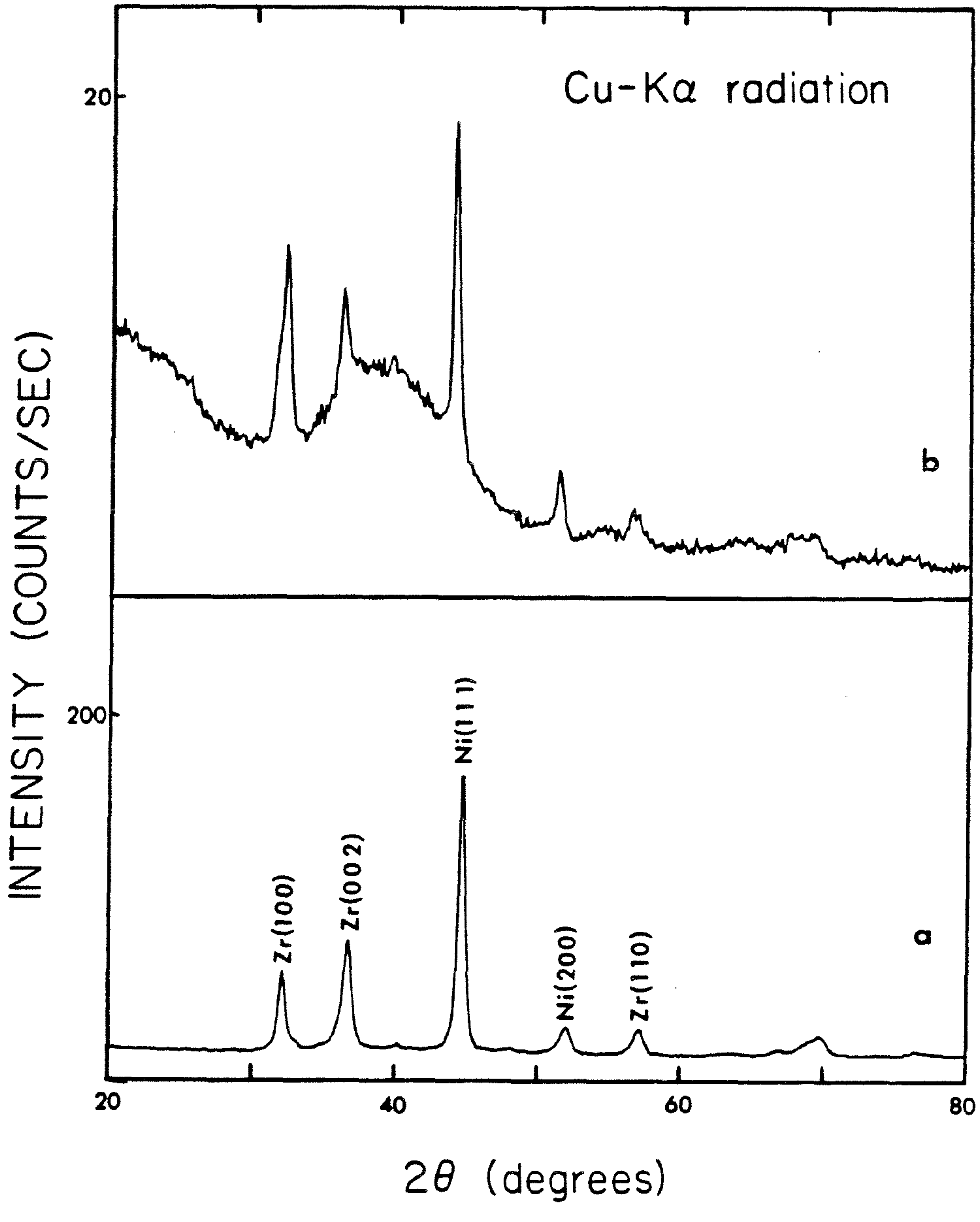

Figure 3.5 X-ray scattering intensity as a function of scattering angle for the samples of Fig. 3.2, measured in transmission geometry.

the present case, there is no known method of estimating it and it will be set equal to one as a first approximation. Line broadening due to small crystal size L (Scherrer broadening)$^{3.8}$ is given by

$$\Delta K = 0.9*2\pi/L \quad ; \tag{3.2}$$

i.e., it is independent of the wavevector K. The full width at half-maximum was measured for a Ni-Zr composite. It was calculated by fitting a Lorentzian to the line and and a 4th order polynomial to the background. The values obtained were corrected for K_α and instrumental broadening (see Ref. 3.9), the latter measured with a single crystal. The result (Fig. 3.6) shows that the dominant contribution to the line broadening is from strains, where $\langle e^2\rangle^{1/2}$ is about 1.5 percent for A=1.

The samples were annealed for 1- 32 hours at temperatures ranging from 250 °C to 370 °C. In Figs. 3.3b and 3.4b, the X-ray patterns are shown for samples reacted as follows: 3.3b: $Ni_{62}Zr_{38}$ 14 hr at 260 °C, 3.4b: $Cu_{60}Zr_{40}$ 8 hr at 275 °C. In both cases, 10 degree broad diffuse diffraction maxima appear in a range of K values, where no Bragg peaks were present before the reaction. These maxima are broader than any observed strain- and size-broadened Bragg peaks and they go up as the intensity of the original Bragg peaks goes down. We therefore attribute them to a growing amorphous phase. The original peaks are reduced in intensity, but are still present; i.e., the reaction is not complete. Attempts to drive the reaction to completion by increasing the time or the temperature resulted in the formation of intermetallic compounds, as manifested in the appearence of new Bragg peaks (Fig. 3.7).

It should be noted that the original Bragg peak intensities do not

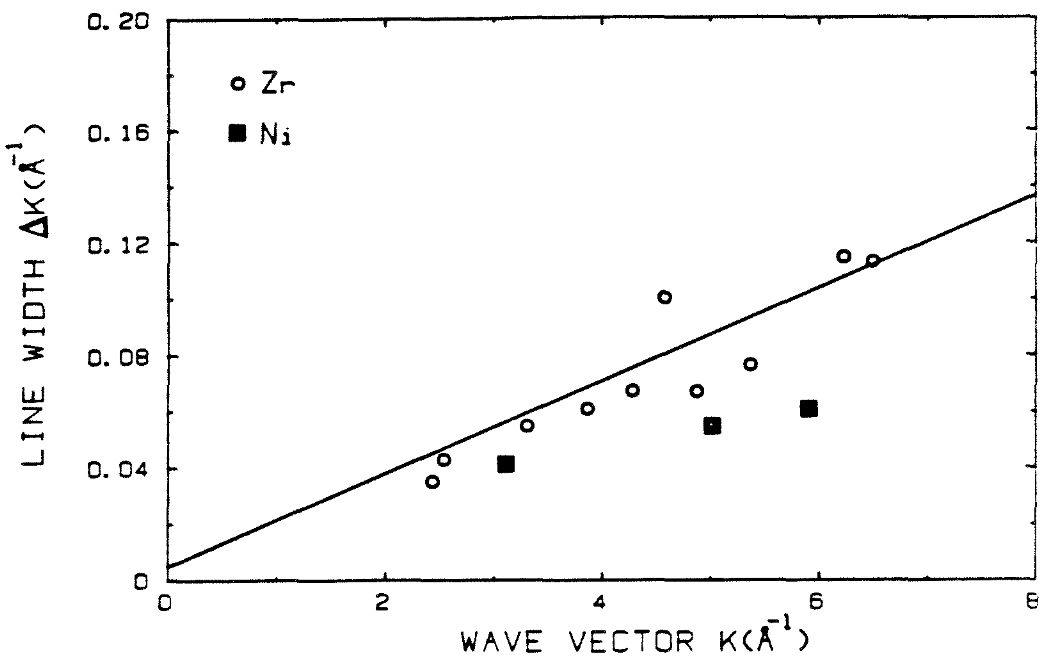

Figure 3.6 Bragg peak broadening ΔK as a function of the magnitude of the wave vector for a Ni-Zr composite deformed in 8 passes.

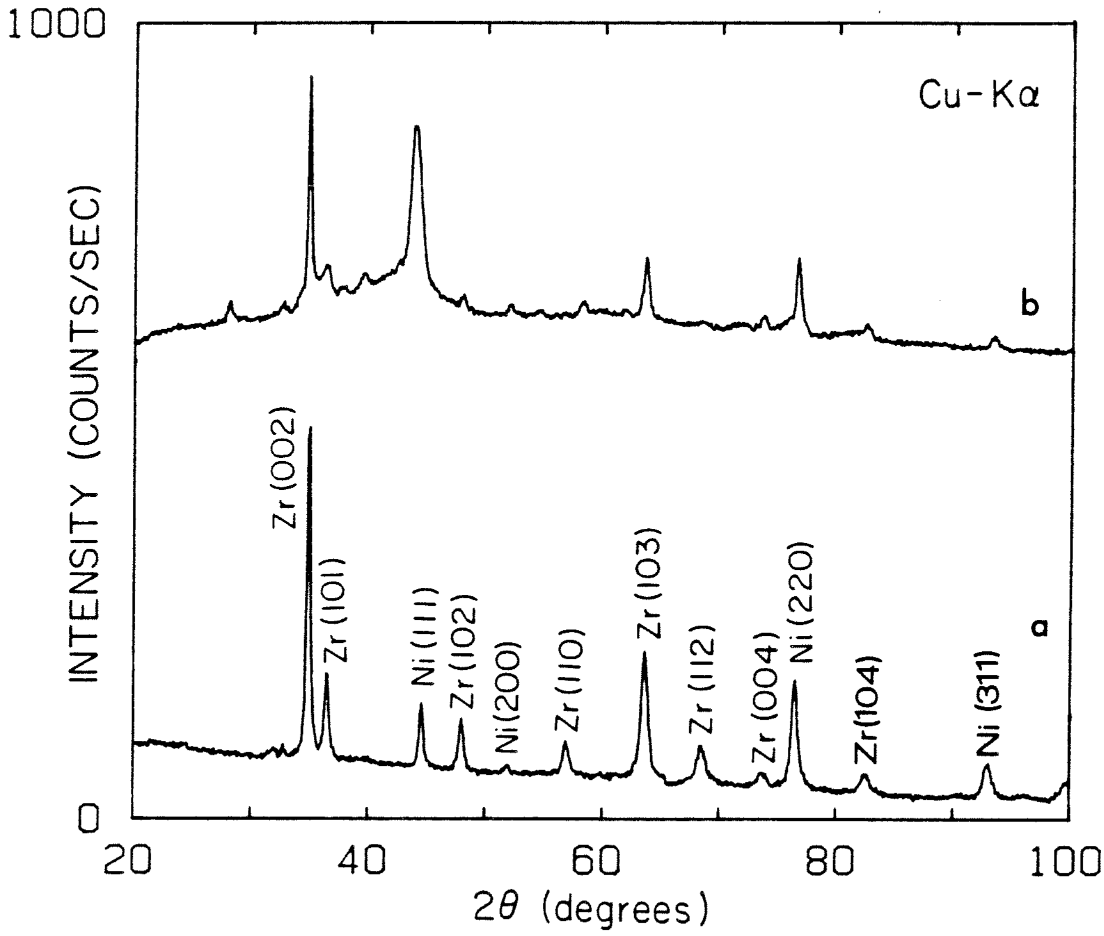

Figure 3.7 X-ray scattering intensity as a function of scattering angle for $Ni_{62}Zr_{38}$ composite reacted at 340 °C for 4 hr.

all decrease at the same rate during the reaction. In the Ni-Zr reaction, the Zr (110) and the Ni (111) showed the fastest rate of decrease while the Ni (220) increased slightly. As verified by separate annealing of cold- worked nickel foils at 260 °C, the latter observation was shown to be related to preferred (220) coarsening of nickel grains . Zirconium was shown not to re-orient at this temperature on the scale of hours.

The crystallization behavior of the alloys obtained was studied by means of DSC. Scans were performed at heating rates of 20 and 40 °C/min with several of the following samples: Ni_xZr_{1-x} (x= 62, 68, reacted at 270 °C for 8 to 16 hr), $Cu_{60}Zr_{40}$ (275 °C for 8 hr). Fig. 3.8 shows scans for a) $Ni_{68}Zr_{32}$, 270 °C for 10 h, b) $Cu_{60}Zr_{40}$, 275 °C for 8 h, both done at a heating rate of 40 °C/min. Separate, severely cold-worked nickel and zirconium foils were scanned to verify that the features observed were not caused by oxidation or recrystallization of the elemental material. For all samples a high exothermic plateau is observed, starting at about 200 °C. In addition, the $Ni_{68}Zr_{32}$ shows a sharp exothermic peak at about 560 °C. For a heating rate of 20 °C/min, the peak is observed between 550 and 560 °C. The $Cu_{60}Zr_{40}$ shows a small endothermic peak superposed on the plateau at 440 °C and two sharp exothermic peaks at 475 °C and 500 °C. An X-ray diffraction pattern of a reacted $Ni_{72}Zr_{38}$ sample heated to 500 °C for 3 min and cooled rapidly shows the presence of amorphous material plus several Bragg peaks of a new crystalline phase, apparently formed from the remaining unreacted elemental material. After annealing at 570 °C for one minute, the diffraction pattern consists entirely of sharp Bragg peaks. The sharp exothermic peak is therefore attributed to the crystallization of the

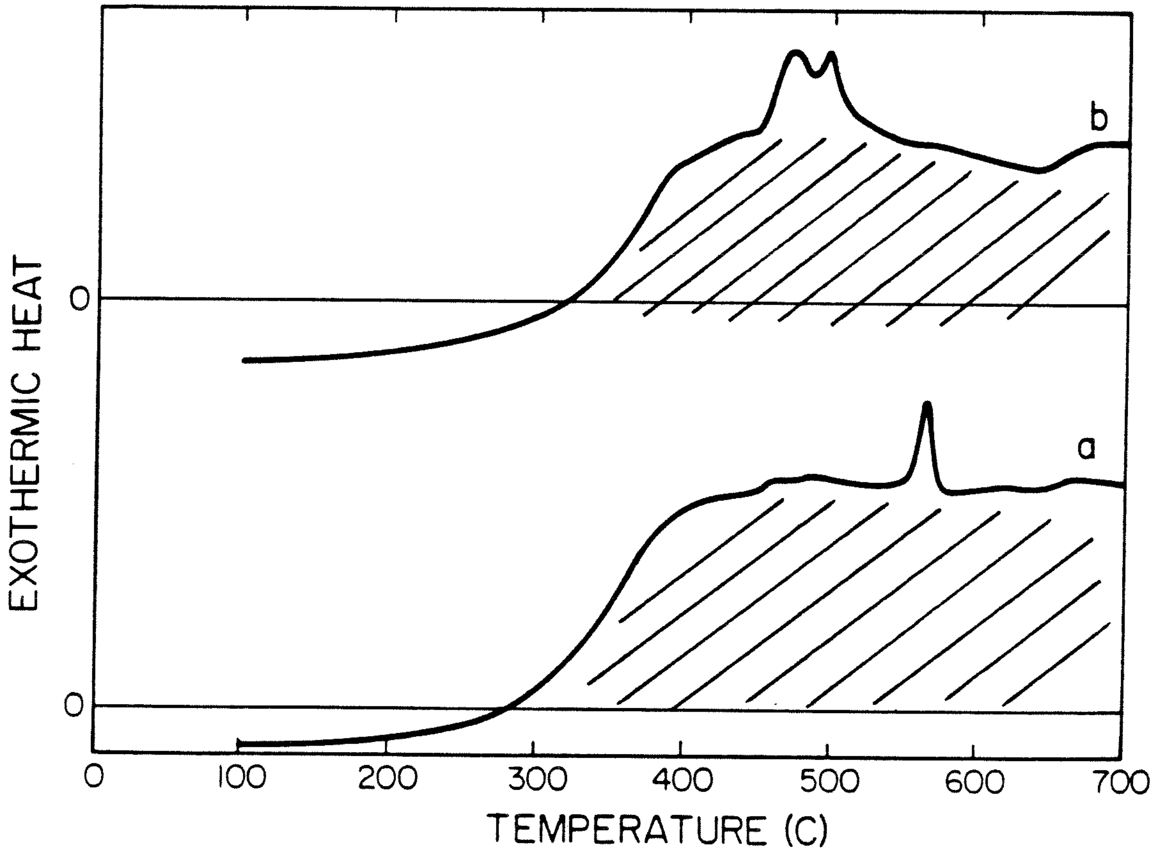

Figure 3.8 DSC scans for $Cu_{60}Zr_{40}$, reacted at 275 °C for 8 hr (top) and $Ni_{68}Zr_{32}$, reacted at 270 °C for 10 hr, both scanned at a heating rate of 40 °C/min.

amorphous phase formed at lower temperatures. The exothermic plateau can be attributed to the completion of the reaction of the elemental phases. It occurs at a temperature higher than the reaction temperature, and results in the formation of crystalline intermetallic compounds. Since the heats of mixing involved are large, the signal obtained is substantial compared to the heat of crystallization of the amorphous alloy (a typical value for the crystallization enthalpy of an amorphous alloy is one kJ/mol).[3.10] Dolgin[3.11] observed a similar behavior in Au-La thin film reaction: in a certain temperature range the amorphous phase, formed at a lower temperature, was stable, but remaining elemental material reacted to form crystalline intermetallic compounds.

3.3 SSR IN ERBIUM-BASED COMPOSITES

Ni-Er and Cu-Er composites were prepared using elemental foils. The number of passes varied from 10 to 55. In Fig. 3.9 and 3.10, the X-ray diffraction patterns are shown for Ni-Er (12 passes) and Cu-Er (14 passes), respectively. The elemental erbium (hexagonal) shows a texture similar to the one observed for zirconium in zirconium-based composites. However, the nickel lines do not show the strong (220) texture observed in Zr-Ni for the same number of passes. The line broadening was plotted vs. the K- value (Fig. 3.11), showing that strain is the dominant broadening mechanism. The rms strain is approximately 2.5 percent.

Samples were annealed between 70 °C and 170 °C for 1- 10 hours. Typical reaction products are displayed in Figs. 3.9, 3.10 for composites deformed in 14 passes. One observes that the Bragg peak intensities decrease upon reaction, and a broad maximum arises from the amorphous phase formed. For Cu-Er composites, the CuEr compound (CsCl structure) appears together with the amorphous phase at all reaction

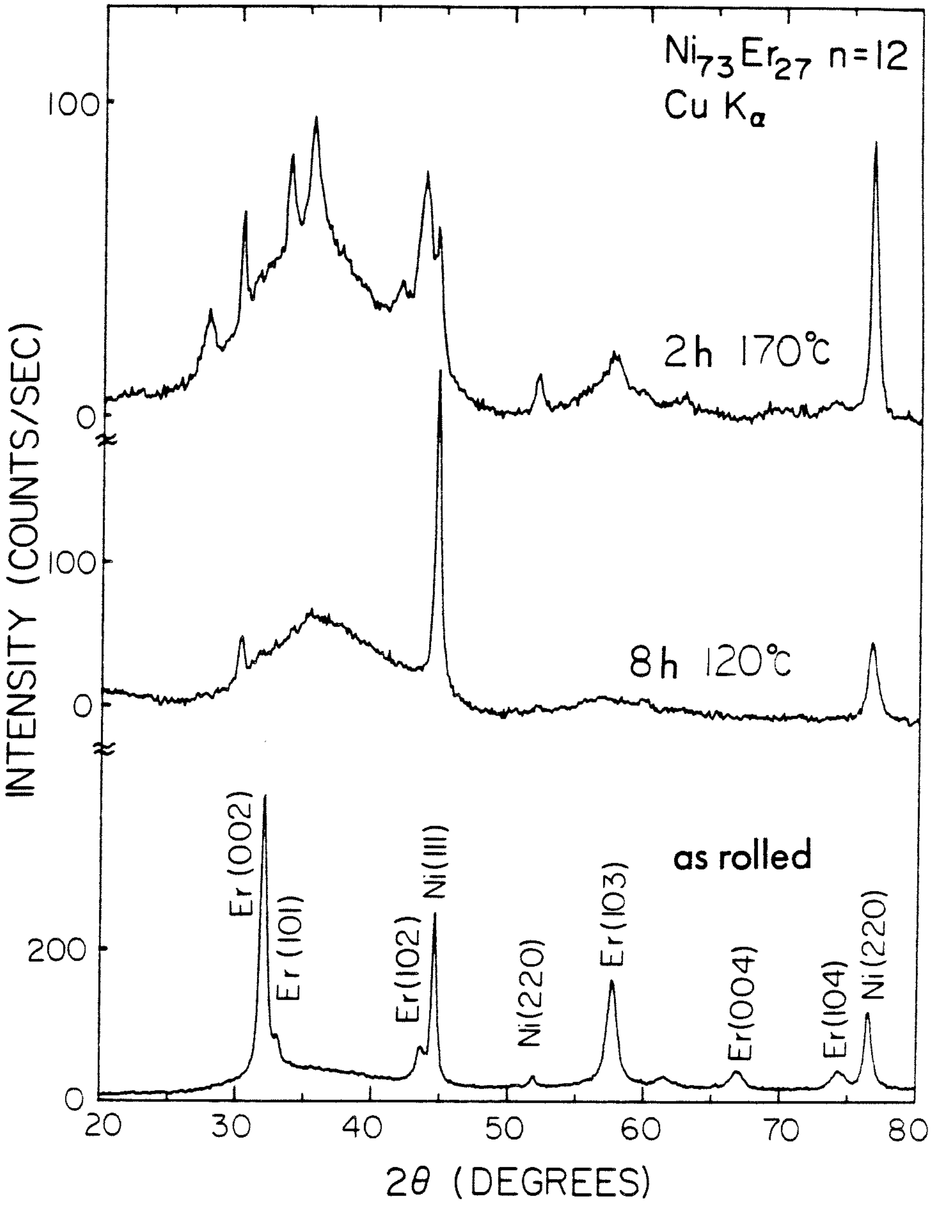

Figure 3.9 X-ray scattering intensity as a function of scattering angle for $Ni_{73}Er_{27}$ (12 passes) as rolled and reacted.

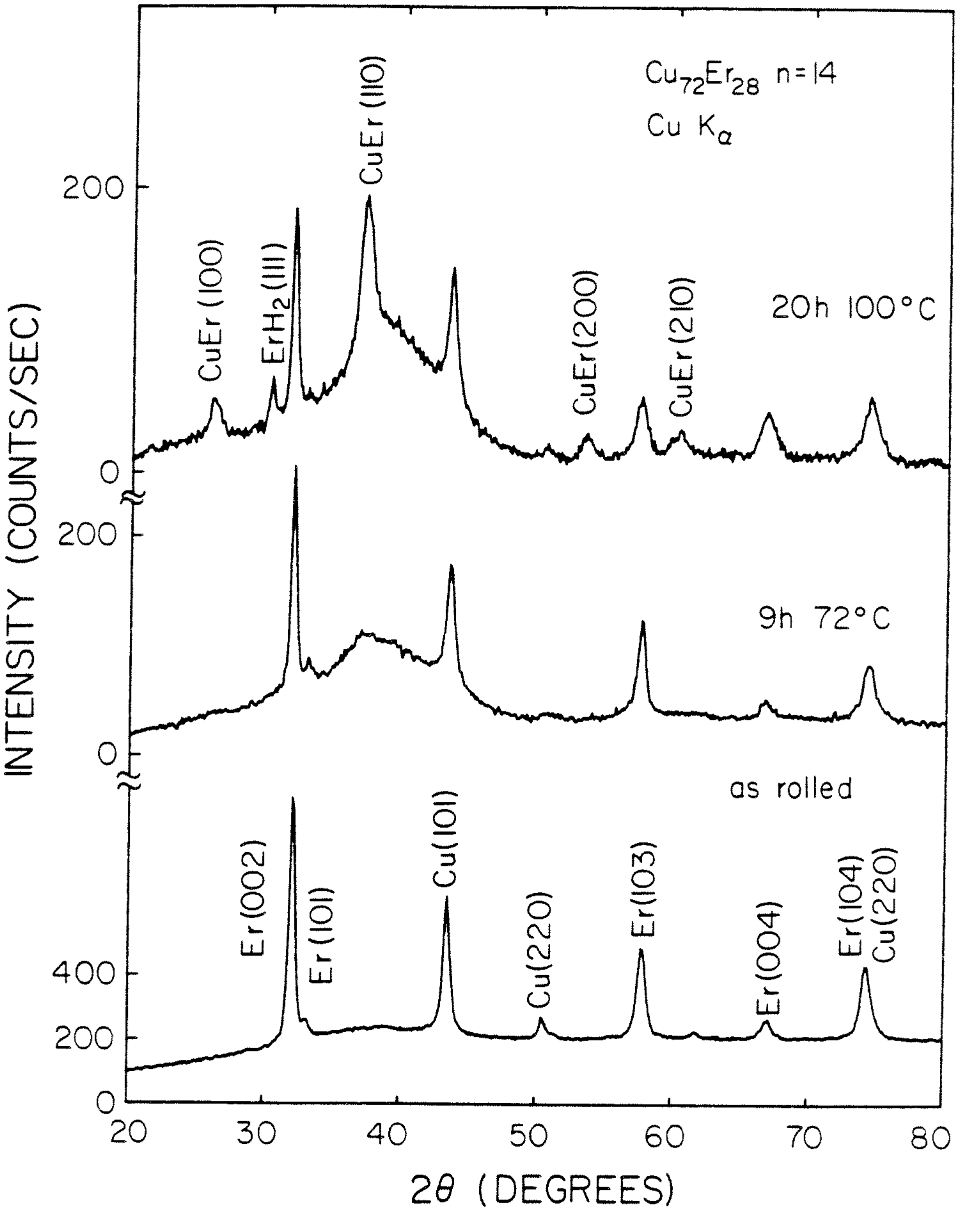

Figure 3.10 X-ray scattering intensity as a function of scattering angle for $Cu_{72}Er_{28}$ (14 passes) as rolled and reacted.

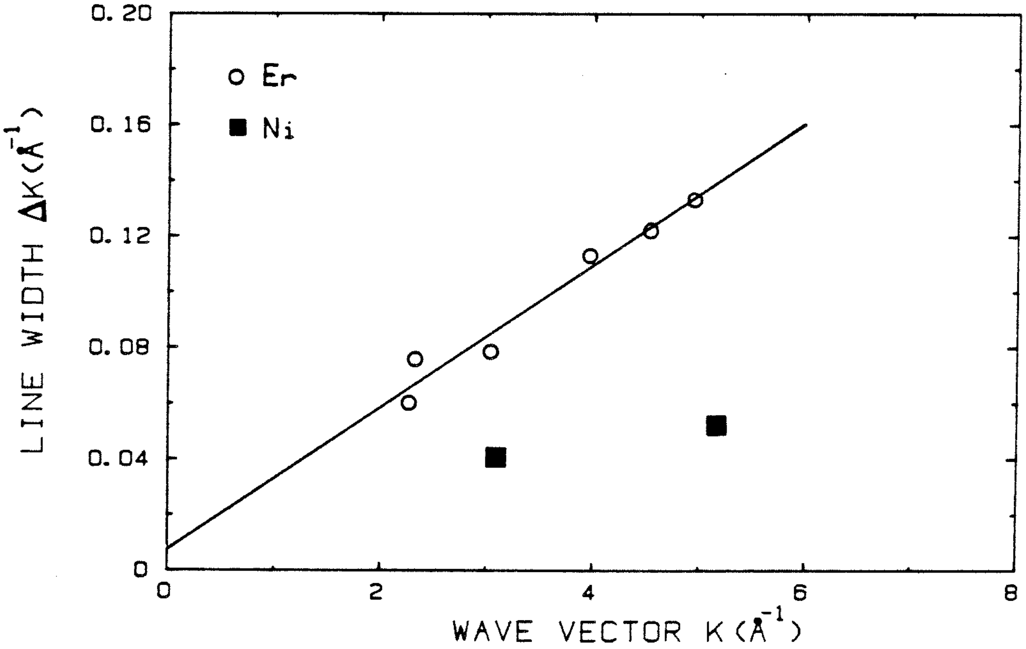

Figure 3.11 Bragg peak broadening ΔK as a function of the magnitude of the wave vector for a Ni-Er composite deformed in 12 passes.

temperatures. It has a lattice parameter of 3.438±0.005 Å, in agreement with the value of 3.43±0.01 Å given in the literature.[3.12] In the Ni-Er reaction, one (or more) unidentified crystalline phase(s) appeared at reaction temperatures above 130 °C. The average composition of the composite and the relative consumption of the constituent elements, as seen from the decrease of the Bragg peak intensities, served as a rough estimate of the composition for the amorphous phase formed. The Cu-Er phase contained approximately 72 atomic percent copper, whereas the Ni-Er phase had approximately 55 percent nickel. In following experiments, samples were prepared at these compositions.

As in the zirconium-based composites, none of the reactions could be brought to completion by thermal treatment. About 20 percent of the original elemental phases were still present after reaction. Increasing the temperature or time resulted in the formation of crystalline intermetallic compounds. The only sample prepared in 14 passes, in which thermal treatment led to complete consumtpion of one phase, was a $Ni_{73}Er_{27}$ composite annealed at 120 °C for 8 hours. The erbium peaks disappeared, and an amorphous phase was observed in addition to remaining nickel (Fig. 3.9). The (111) peak of ErH_2 was also seen (see next paragraph).

Complete amorphization was achieved for $Ni_{72}Er_{28}$ and $Cu_{55}Er_{45}$ by continuous deformation through 40- 55 passes (Figs. 3.12, 3.13) The sample temperature during deformation did not rise above 40 °C, and fell off to 30 °C over a period of 100 msec (see Fig. 3.14). Upon reaction, Bragg peaks corresponding to face-centered cubic ErH_2 appear in both alloys, with a lattice constant of 5.125±0.005 Å. In the literature, the value is given as 5.123 Å.[3.12] The use of distilled erbium with less than

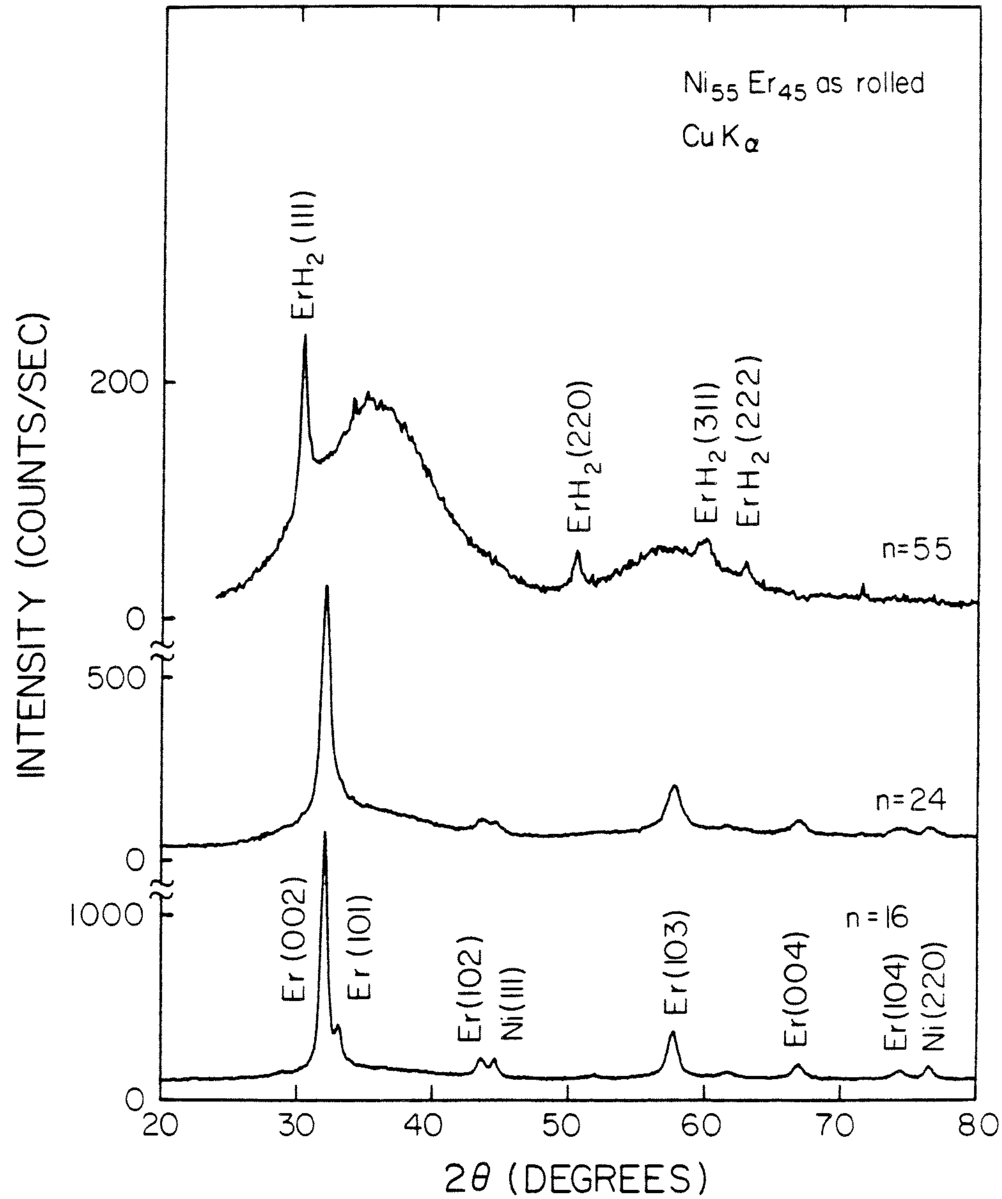

Figure 3.12 X-ray scattering intensity as a function of scattering angle for $Ni_{55}Er_{45}$ at different numbers of deformation passes n.

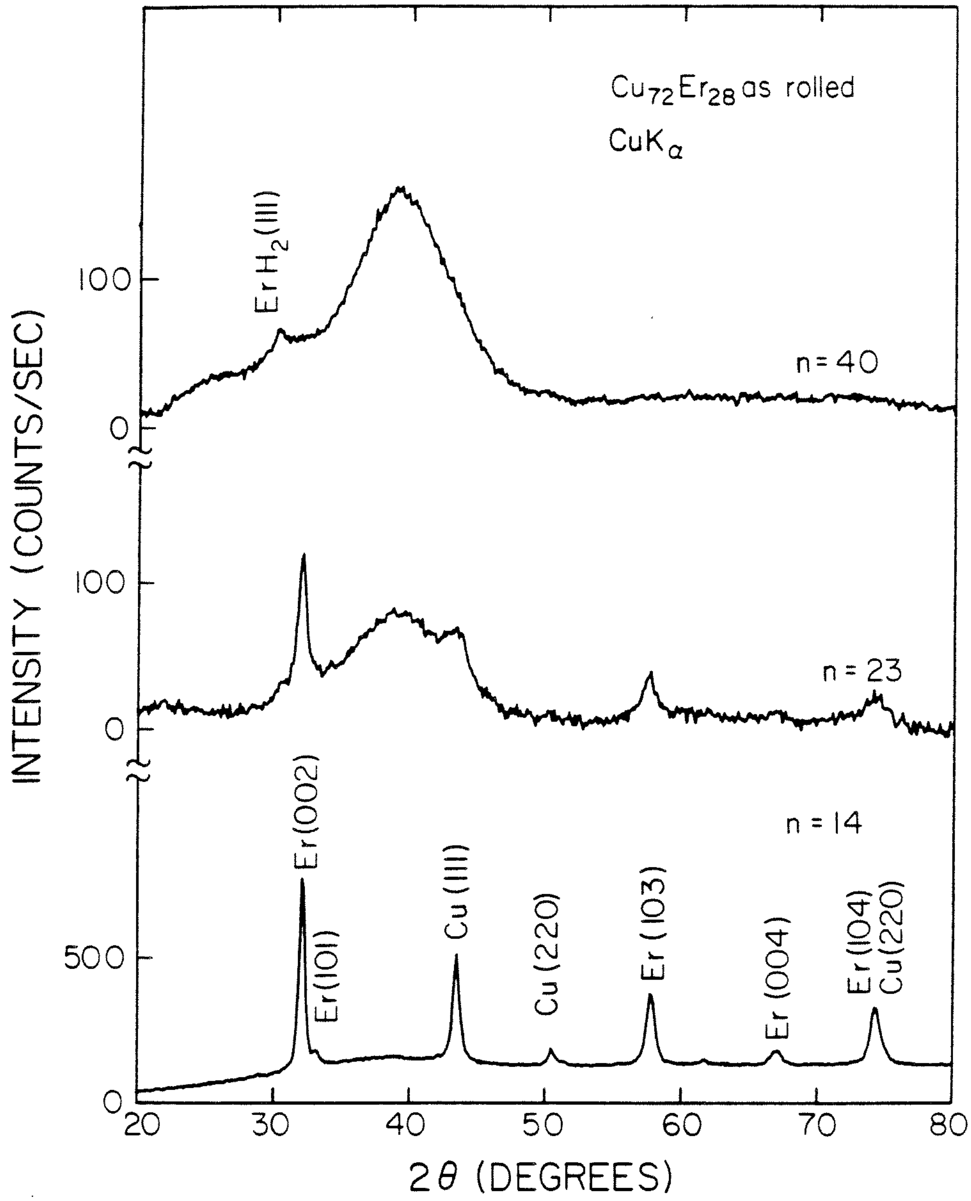

Figure 3.13 X-ray scattering intensity as a function of scattering angle for $Cu_{72}Er_{28}$ at different numbers of deformation passes n.

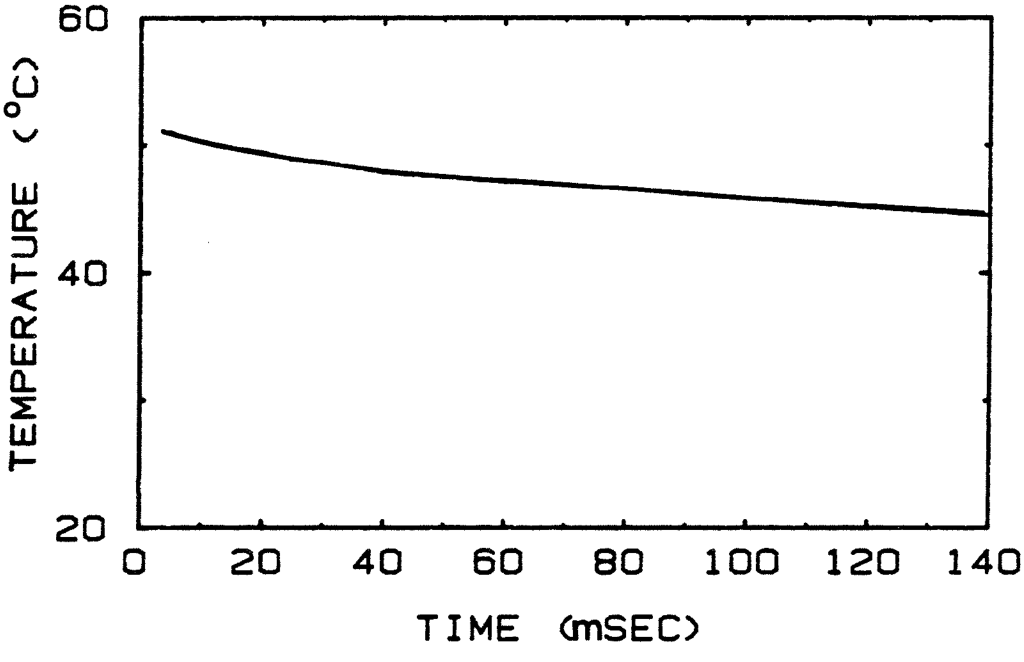

Figure 3.14 Temperature as a function of time during deformation of Ni-Er composite.

0.1 atomic percent hydrogen resulted in a product with substantially lower hydride peaks. This indicates that the hydrogen originates from the erbium as a dilute impurity.

In order to compare the amorphous alloy produced by cold rolling to the corresponding alloys produced by conventional rapid cooling methods, attempts were made at several preparation methods. Neither of the three liquid-quenching methods described in Chapter 1 produced a completely amorphous $Cu_{72}Er_{28}$ alloy. The best result was obtained in a single foil (out of 20) produced by the piston and anvil method, which contained only several percent (unidentified) crystalline material, as seen by X-ray diffraction (Fig. 3.15). This sample foil was used for DSC runs. The same alloy was produced in a pure amorphous phase by magnetron sputtering. The foils were $\cong 10$ μm thick and could be removed from the Pyrex substrates with a sharp blade. They were used for DSC and several foils were stacked and glued with diluted Duco- cement to produce a 60 μm thick sample for an RDF measurement. A comparison of the reduced interference function K(I(K)-1) and radial distribution function G(r) obtained from rolled and sputtered $Cu_{72}Er_{28}$ is shown in Figs. 3.16 and 3.17.

In Fig. 3.18, DSC scans are shown for amorphous $Cu_{72}Er_{28}$ produced by rolling, liquid-quenching and sputtering. The alloy produced by rolling shows a sharp crystallization peak centered at 367 ^{o}C. By heating samples to temperatures above and below the peak and comparing them by X-ray diffraction, the peak was verified to be a result of crystallization. The sputtered and liquid-quenched alloys both also showed exothermic peaks, at 352 ^{o}C and 371 ^{o}C, respectively. The liquid-quenched alloy also showed a tail on the lower temperature side of the

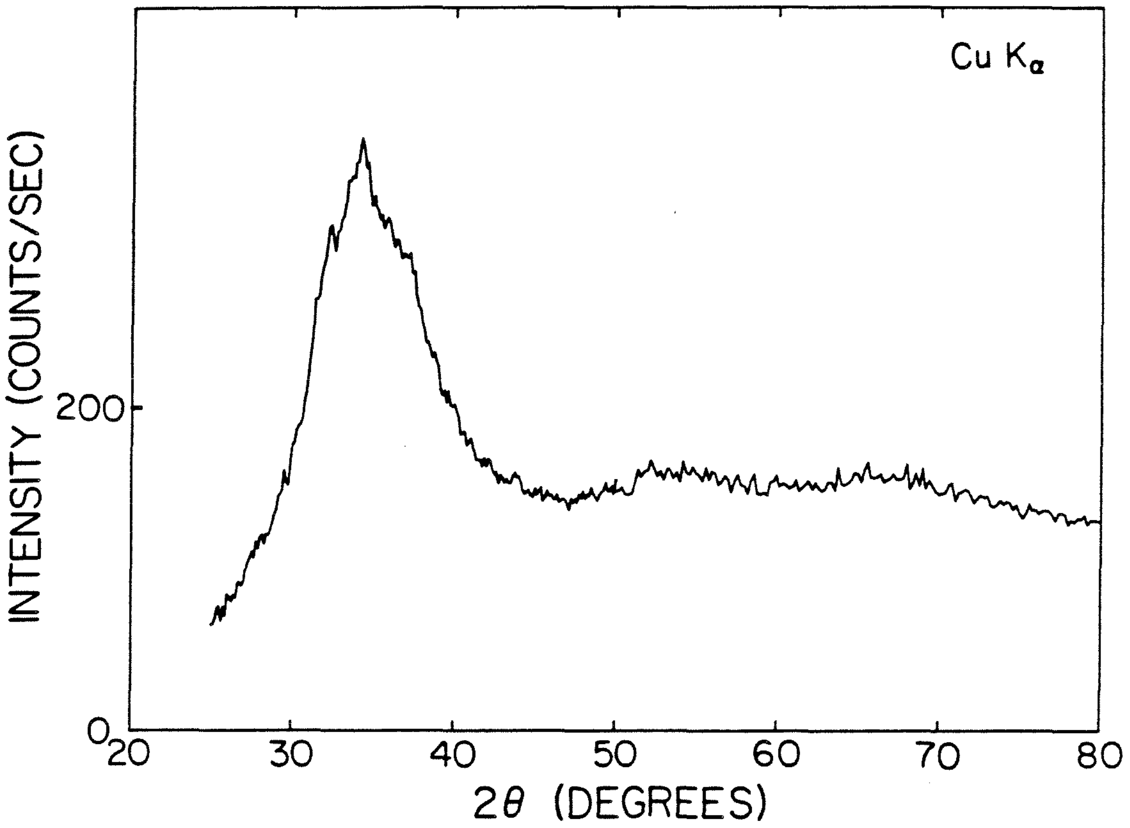

Figure 3.15 X-ray scattering as a function of scattering angle for a $Cu_{72}Er_{28}$ foil prepared by rapid quenching. Sharp features indicate presence of a small percentage of crystalline material.

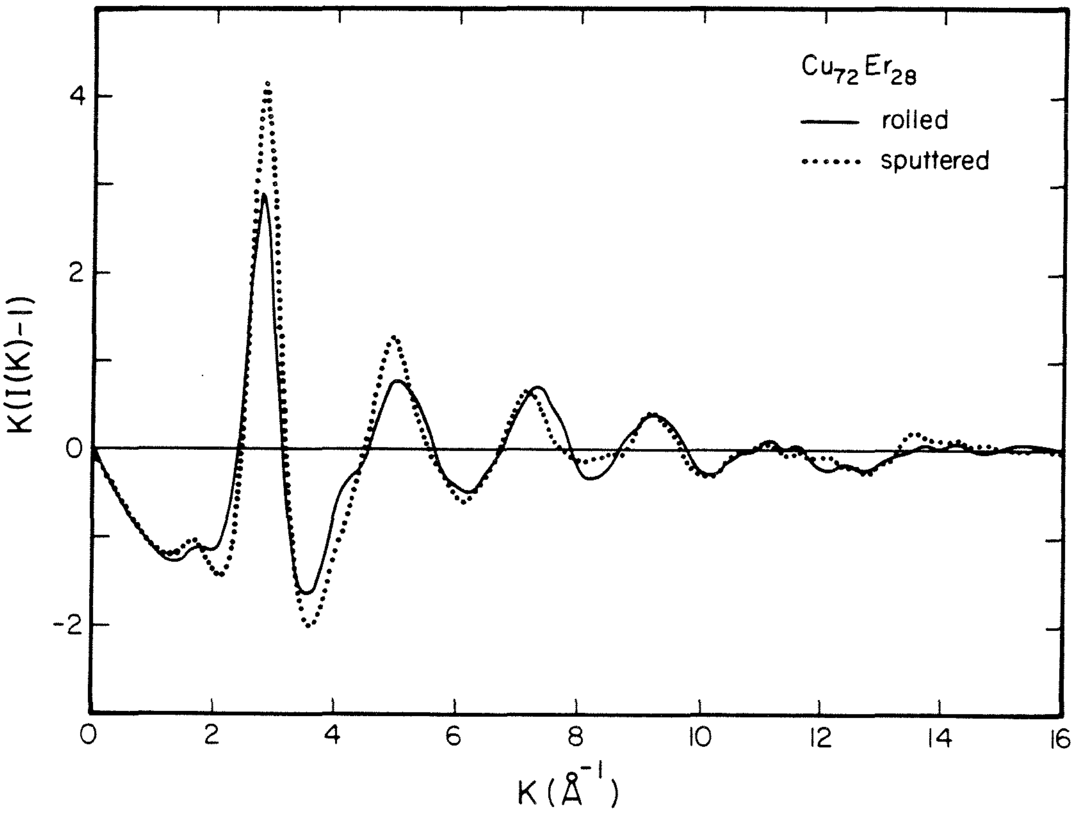

Figure 3.16 Reduced interference function as a function of the magnitude of the K- vector for amorphous $Cu_{72}Er_{28}$ prepared by rolling and sputtering.

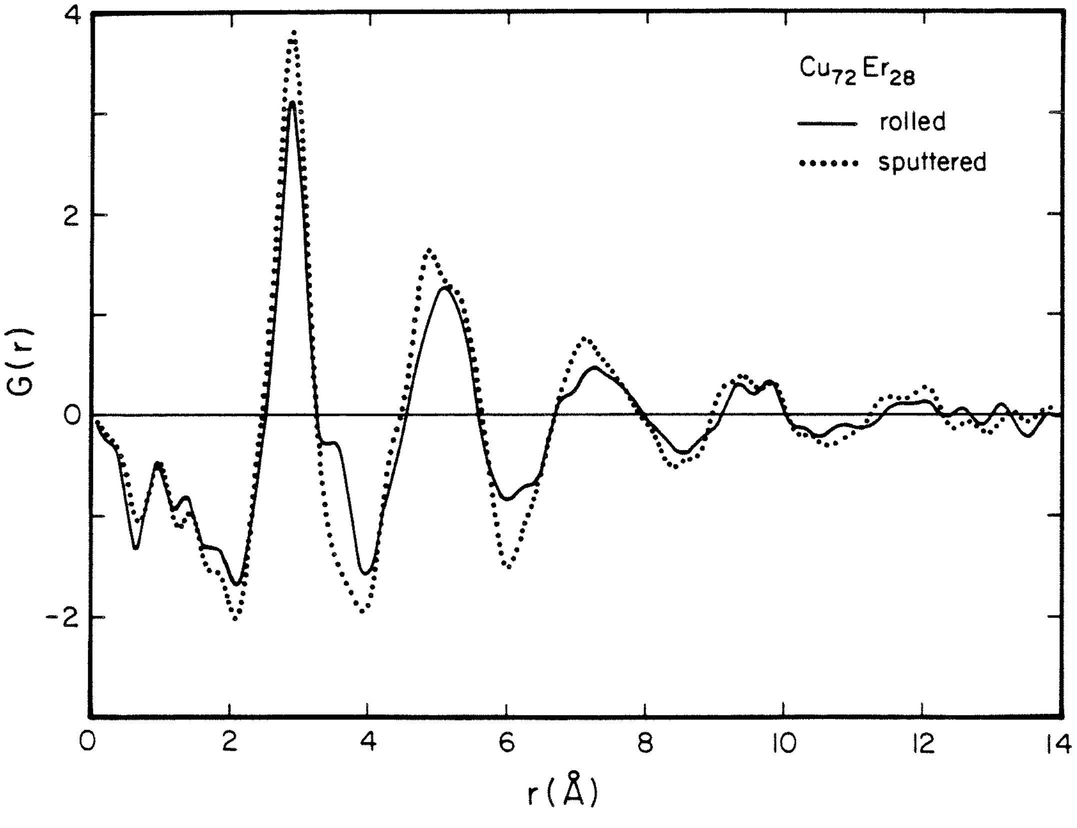

Figure 3.17 Reduced radial distribution functions for amorphous $Cu_{72}Er_{28}$ prepared by rolling and sputtering.

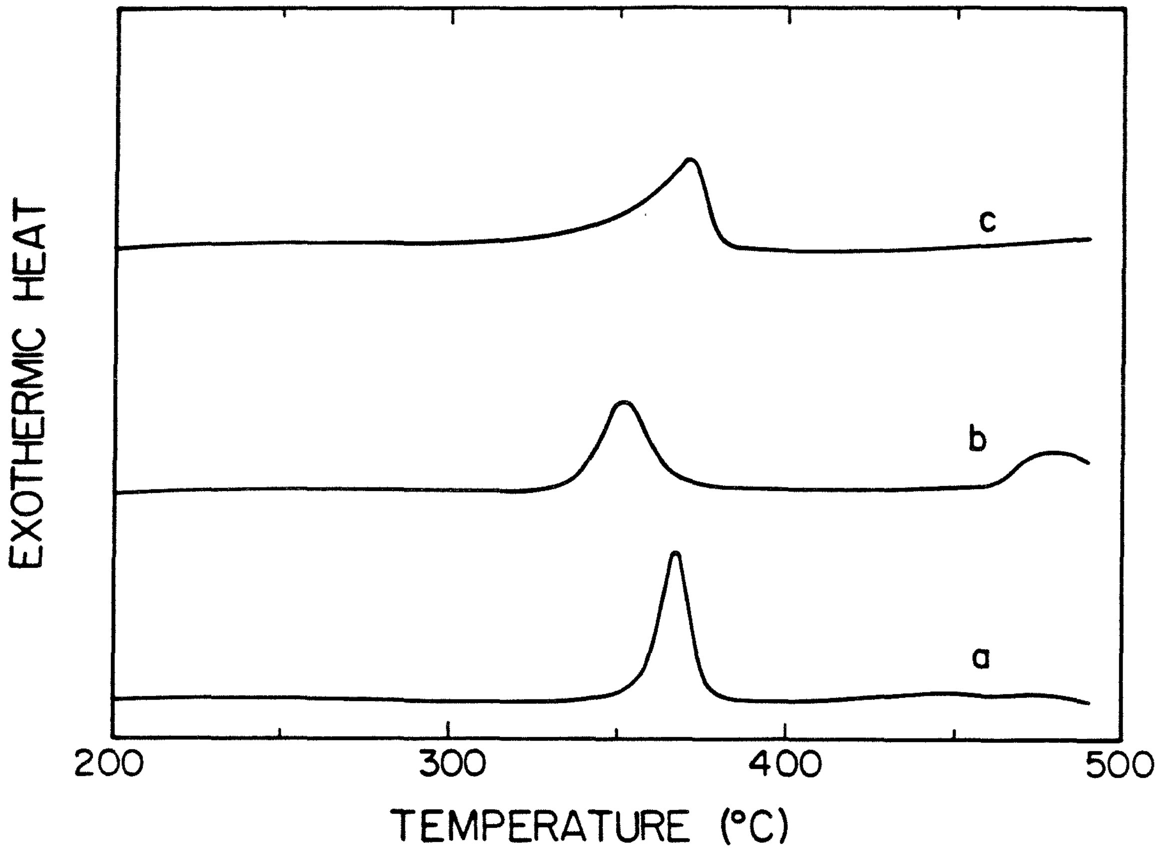

Figure 3.18 DSC scans at 40 °C/min for amorphous $Cu_{72}Er_{28}$ prepared by (a) rolling, (b) sputtering, (c) rapid quenching. Sample (c) contains a small percentage of crystals.

peak. Since it contained a small fraction of crystals, the tail can be attributed to growth of these already present nuclei at temperatures below that required to form the nuclei homogeneously. A similar observation was made by Dong et al.,[3.13] who reported that partially crystallized amorphous Ni-Zr alloys show a crystallization peak at the same temperature as the fully amorphous alloys, in addition to an exothermic signal at lower temperatures. All three alloys show second exothermic events above 400 °C , but they differ considerably. It should be noted that the sample produced by rolling showed the sharpest crystallization peak. Amorphous $Ni_{55}Er_{45}$ prepared by rolling crystallized at 276 °C at a heating rate of 29 °C/min.

3.4 DISCUSSION

3.4.1 Formation and Characterization of The Amorphous Phases

For both Zr- and Er- based composites, the amorphization reaction could not be completed by thermal treatment. Typically, about 20 percent of the original material did not react even after extended times, and crystalline compounds formed. Several possible explanations can be suggested. Surface contaminants present on the starting material are distributed on the interfaces in the composite after deformation and act as diffusion barriers. For composites made by the powder- metallurgical method, there are finite probabilities for grains of the same species to be in contact with each other. This will cause a corresponding increase in the size of the layers in the final composite. For diffusion controlled growth , the reaction time will increase as the square of the layer thickness. For samples deformed in 12 passes, one would expect a reduction of $2^{12} \cong 4000$ if the deformation is uniform. If the initial thickness is 20 μm, it becomes 50 Å in the final product. However, the deformation process is not uniform and there is a distribution of layer thicknesses. Since the composite foils embrittle as a result of the cold working, every time a foil is folded, it does not overlap itself completely. In a simple model, we assume that in each pass, a randomly located area, which constitutes 10 percent of the sample does not overlap any other part of the sample. This area is assumed not to be deformed in the subsequent pass. As can be proven by induction, the resulting thickness distribution is given by

$$p_m^n = \binom{n}{m}(0.9)^m(0.1)^{n-m} \tag{3.3}$$

where p_m^n is the fraction of the material reduced by 2^m after n passes ($n \geq m$). For n=12, 0.5 percent of the sample is deformed by a factor of $2^7 = 128$ to a size of ≈1600 Å. The time needed to react such a layer would be 16 times longer than for a 400 Å thick layer, allowing the nucleation of crystalline compounds. In conclusion, the above arguments, in addition to the fact that crack formation causes nonuniform deformation, imply a broad distribution in the layer thicknesses. During the time period necessary for the reaction of the thick layers, crystalline intermetallic compounds can nucleate and grow.

The textures observed for the hexagonal metals correspond roughly to the reports in the literature, with the close- packed plane (002) parallel to the foil surface. For the fcc metals, the nickel in Ni-Zr shows strong (220) texture, in correspondence with Ref. 3.6. In Ni-Er, such a strong texture is not observed, possibly due to the fact that Zr has a yield stress higher than erbium. The copper in both Cu-Er and Cu-

Zr does not show noticeable texture.

The DSC data suggest nearly identical thermal behavior for amorphous alloys produced by rapid cooling from the melt and by SSR. For Ni_xZr_{1-x}, Dong et al.[3.13] report a maximum of about 575 °C for the crystallization temperature (T_x) as a function of composition at x = 64 atomic percent nickel. Our value of T_x = 560 °C for $Ni_{68}Zr_{32}$ lies close to this value. For $Cu_{60}Zr_{40}$, the endothermic peak at 440 °C indicates a glass transition, which is the definitive indication for a glass. As is usually observed, the signal is very small, but it can be reproduced and is not a result of random noise. Here again, there is a good correspondence with Kerns et al.,[3.14] who report T_g = 440 °C and T_x = 490 °C for rapidly quenched Cu_xZr_{1-x} alloys of similar composition. For the erbium based alloys, the complete amorphization made possible a higher quality measurement of the thermal behavior. Fig. 3.18 shows the similarity in the crystallization behavior of $Cu_{72}Er_{28}$ alloys prepared by three different methods, with the measurements done at identical conditions. For the liquid-quenched alloy (which contained crystalline material), the shoulder on the low temperature side of the crystallization peak is a result of growth of already present heterogeneous crystalline nuclei. Dong et al.[3.13] made a similar observation on a partially crystallized amorphous Ni-Zr alloy. They observed a crystallization peak at the same position as for the completely amorphous sample, and an additional peak at slightly lower temperature. This can be understood as a crystallization process (homogeneous or heterogeneous) which ocurs in the amorphous matrix independent of previous partial crystallization on the nuclei present. The crystallization temperatures of the liquid quenched and the rolled sample lie within 4 degrees of each other, and the sputtered sample crystallizes at a temperature 15 degrees lower than the rolled one. The latter difference could be a result of argon trapped in the sputtered films or of composition variations. The secondary crystallization events which take place at higher temperatures show considerable differences among the three samples. This could be a result of different impurities and textures present after the first crystallization events. Since for amorphous alloys with high heats of mixing, the crystallization temperature depends strongly on the the composition,[3.13] the sharpness of the crystallization peak indicates that the sample produced by rolling is chemically homogeneous by the time its temperature approaches T_x.

Additional evidence for the similarity of the amorphous alloys prepared by sputtering and rolling is the comparison of their atomic structure, as seen in the RDF (Fig. 3.17). Up to four nearest-neighbor shells lie at the same radius from the atom at the origin. For the rolled sample, the shoulder on the first peak at 3.63 Å corresponds to Er-Er distances (the Goldschmidt radius of erbium is 1.78 Å). In fcc ErH_2, the Er-Er distance is 3.624 Å. The shoulder is believed to be due to a contribution of the Erbium hydride present in the sample. This assumption is based on the fact that for a sample containing a higher percentage of ErH_2, this shoulder was more pronounced and peak-shaped, and its intensity could be reduced by partial subtraction of the ErH_2 Bragg peaks from the scattered intensity I(K). For the sputtered sample, the peaks and minima in G(r) are less pronounced than in the rolled sample. This could be explained by the fact that the sputtered sample is more relaxed. In general, sputtered samples are less relaxed than liquid quenched ones because of their higher effective cooling rates,[3.15] but the amorphous $Cu_{72}Er_{28}$ alloy has a relatively low crystallization temperature and therefore it relaxes at the temperature it reaches during deposition, about 80- 100 °C. Attempts to relax the rolled alloy at 115 °C did not change the RDF, and we attribute the difference in the RDF's to the fact that the rolled sample had a rough surface, which caused a reduction of the scattered intensity at small angles by shadow effects. A quantitative correction for this effect is possible only for a well-defined shape of the surface.

In all SSR experiments reported to date, formation of crystals is favored over amorphization as the temperature is increased. This indicates that the temperatures were below the "nose" of Fig. 1.6. It also implies that the activation energy for the formation of a crystalline nucleus is higher than that of an amorphous nucleus.

3.4.2 Thermal Effects During Sample Preparation

Since in copper- erbium composites, interdiffusion was observed after 10- 14 deformation passes at temperatures as low as 70 °C, it is important to analyze the heating effects during mechanical deformation. In addition to the measurement of temperature values, an attempt will be made to estimate the heat evolved during the deformation.

The measurement of the temperature of a composite during its deformation shows that it rises to ≅40 °C and falls off on a scale of several msec (Fig. 3.14). Since the whole preparation process involves about 10^3 steps, we see that the total time is shorter and the temperature lower than the respective values at which samples were reacted after intermediate deformation.

In order to calculate the heating effect, we will first show that the heat deposition is uniform throughout the sample. We assume the extreme case that heat is deposited only at the interfaces and show that the thermal relaxation time is shorter than the duration of the deformation. Fig. 3.19 illustrates the deformation process. The sample thickness is reduced by $2x \cong 5 * 10^{-3}$ cm each time it passes between the rollers. The angle α is given by

$$\cos\alpha = (r-x)/r \quad ; \qquad (3.4)$$

i.e.,

$$\alpha = 0.0258 \text{ rad} .$$

The duration of the deformation is given by

$$t = \frac{\alpha}{\omega} \simeq 5 \text{ msec} \qquad (3.5)$$

where is the rotation frequency of the rollers

$$\omega = 2\pi/1.2 \text{ sec}^{-1} .$$

If the temperature is a delta function in one dimension at the time t=0, its time and position dependence are given by[3.16]

$$T(x,t) = \frac{1}{4\pi\kappa t} \exp\left(-\frac{x^2}{4\kappa t}\right) \qquad \left(\kappa = \frac{K}{C\rho}\right) \qquad (3.6)$$

where K is the thermal conductivity, C, the heat capacity and ρ, the density of the material. The relaxation time $\tau_{1/e}$ will be defined as the

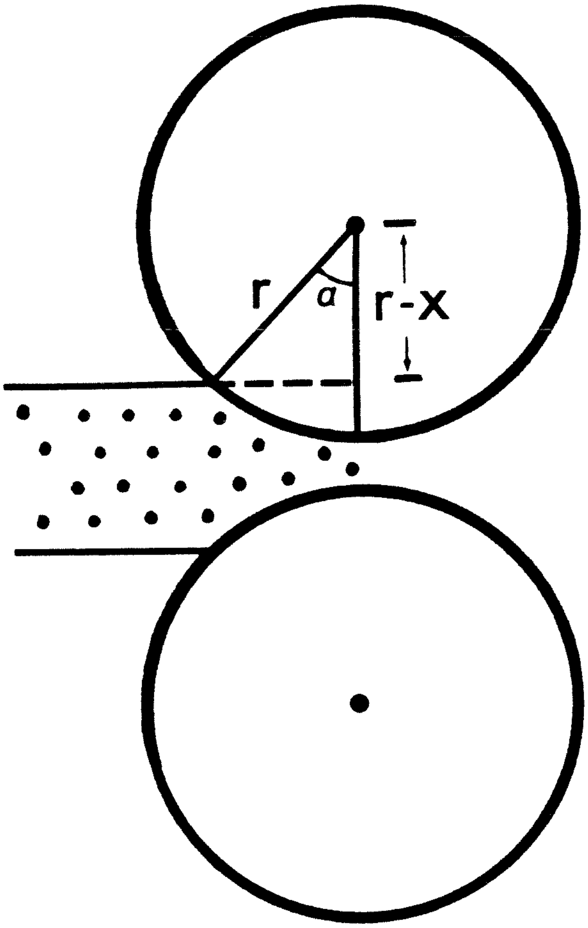

Figure 3.19 Geometry of deformation in a rolling mill.

time it takes the temperature at a distance x from the origin to reach 1/e of its value at the origin. We assume a delta function at each interface and the relevant distance x is half the layer thickness, x = 10 μm for the initial composite.

$$\tau_{1/e} = \frac{x^2}{4\kappa} \tag{3.7}$$

For erbium, $K = 0.023$ cal/(sec cm K)

$C \cong 0.1$ cal/(°K g)

$\rho = 9.0$ g/cm^3

and we obtain $\tau_{1/e} \cong 2.5 * 10^{-6}$ sec .

For copper and nickel the result is smaller, for copper by an order of magnitude. We see that this result is three orders of magnitude lower than the duration of the deformation. The time constant $\tau_{1/e}$ decreases as the square of the layer thickness, so we are safely in the regime of uniform heat deposition. The heat conductivity of single crystals was used, but correcting for the lower conductivity of cold-worked polycrystalline or amorphous metals will increase $\tau_{1/e}$ by one order of magnitude and will not change the general picture.

For plastic deformation, the stress σ is approximately constant and independent of the strain e. Therefore, the deformation energy is given by the product

$$U = \sigma e \quad . \tag{3.8}$$

We shall use the theoretical limit for the yield stress

$$\sigma = E/10 \tag{3.9}$$

given by Dieter,[3.17] where E = Young's modulus. This estimate is based on moving a whole lattice plane at the same time, with no dislocations present to facilitate the deformation. Using $E \cong 10^7$ N/cm^2 for copper or erbium, we obtain $= 10^6$ N/cm^2. The strain caused by the rolling mill in each cycle is approximately 3 percent, so the energy increase due to deformation is

$$U = \sigma e \cong 2000 \text{ J/mol.}$$

Assuming that all the energy is converted to heat, we obtain an increase in temperature:

$$\Delta T = U/C = 80\ {}^{\circ}\mathrm{C}$$

where $C = 25$ J/($^{\circ}$K mol) is the Dulong- Petit value of the heat capacity of a solid. This result is consistent with the measured values, since it is based on the theoretical limit for the yield stress, and gives the upper limit for the increase in temperature.

In addition to the above, we can estimate the increase in the temperature of the stainless steel surrounding the sample. The yield stress for cold-rolled steel is approximately 10^9 N/m^2,[3.18] the strain e = 3 percent and the deposited energy is equal to

$$U = \sigma e = 30\ \mathrm{J/cm^3} \cong 200\ \mathrm{J/mol}$$

and the heating

$$\Delta T = U/C \cong 8\ ^{\circ}\mathrm{C} \quad .$$

This value lies close to the temperature to which the sample temperature is observed to relax after several msec.

In conclusion, we showed that based on measurements, as well as on calculations, the sample temperature during deformation does not increase by more than 20-30 °C, and it relaxes on the scale of 100 milliseconds. The number of cycles per sample is about 10^3, making the total time at elevated temperatures about 2 min. The times and temperatures are therefore considerably below those at which samples with intermediate deformation ratios were reacted (Figs. 3.9, 3.10). We believe that the reaction is possible under these conditions because of the substantial decrease in the thickness of the crystalline layers. In addition, diffusion might be enhanced by the strains during the deformation process. Direct information about the layer morphologies could be gained by electron microscopic studies.

3.4.3 Additional Thermodynamic Parameters

In the above section, we came to the conclusion that there are no substantial heating effects during the sample deformation, and that the amorphization is driven at room temperature by the chemical heat of mixing of the constituent elements. The layer thickness is sufficiently small (or the interface density is high), so that the reaction rate is high at the given temperature.

At the given interfacial densities, however, one has to consider the effect of the interfaces on the total balance of the free energy. When the ratio of surface to volume becomes high, the thermodynamic data derived for bulk materials have to be modified. An interesting case was reported by Willens et al.,[3.19] who observed the depression of the melting point of thin lead films, when the thickness approached tens of Angstroms.

In our case, the free energy of the crystalline material in the composite is raised by the high concentration of defects and interfaces. We can use the value obtained for the rms strain in erbium $\langle e^2\rangle^{1/2} = 2.5$ percent and estimate the strain energy

$$U_{strain} = 1/2 \langle e^2\rangle E \tag{3.10}$$

where Young's modulus E is used as an approximation for the elastic constants involved. One obtains

$$U \cong 0.24 \text{ kJ/mol} \quad .$$

For copper and nickel, the measured $\langle e^2\rangle$ is lower, and U will be of the same order of magnitude.

In order to estimate the interfacial free energies, we use the tabulated values of high-angle grain boundaries. We shall ignore the fact that they apply to grains of the same material, but correct for chemical interactions. The total free energy of an interface will be given by :

$$g_{int} = g_{gb} + g_{ch} \tag{3.11}$$

where the first term is the grain boundary contribution and the second is the chemical correction. We assume the presence of interfaces at spacings of 50 Å, so the interfacial area is $2*10^6$ cm^2 per cm^3. Typical values for the free energies of high-angle grain boundaries are $6*10^{-5}$ J/cm^2;[3.20] i.e., the total free energy is 120 J/cm^3, or approximately:

$$g_{gb} \doteq 0.8 \text{ kJ/mol.}$$

We can try to estimate the reduction of this positive value by chemical interactions with a quasi- chemical approach.[3.21] For alloys with large heats of mixing, typical values are 80 kJ/mol for the 1:1 compounds, and the entropy term in the free energy is negligible. Assuming 8 unlike nearest neighbors per atom and complete chemical ordering, the energy per bond is

$$h = 80/(8*N_A) \text{ kJ} \tag{3.12}$$

where N_A is Avogadro's number. We shall assume z unlike nearest neighbors for an atom on the interface (z = 3-6). The total chemical energy for an interface is approximately

$$g_{ch} = zh/(4r^2) \text{ kJ/cm}^2 = z*0.37 \text{ kJ/mol} \tag{3.13}$$

for the given density of interfaces. r is the atomic radius.

The total free-energy of the interfaces is the sum of the (negative) enthalpy of mixing and the free energy of the grain boundaries. It is hard to predict the sign of this sum, since both terms are about the same order of magnitude. In any case, the sum is on the order of 1 kJ/mol or less.

In conclusion, we see that the values obtained for strain and interfacial free energies are on the order of one kJ/mol, whereas the free energies of mixing are typically tens of kJ/mol. Therefore, the bulk treatment of the free-energy balance is still valid. As an experimental test, a composite was made from Cu and Nb. In liquid CuNb, the enthalpy of mixing is +3 kJ/mol,[3.2] so from bulk free energy considerations, the elements should not mix. Indeed, after deforming the composite in 35 passes, there is no evidence of the formation of an amorphous phase (see Fig. 3.20). For Cu-Er, such a phase formation was observed after 20 passes.

One could speculate that the transient strains caused during the deformation of the composites enhance the interdiffusion between the layers. This could be confirmed by measuring the rate of reaction as a function of stresses applied to a sample.

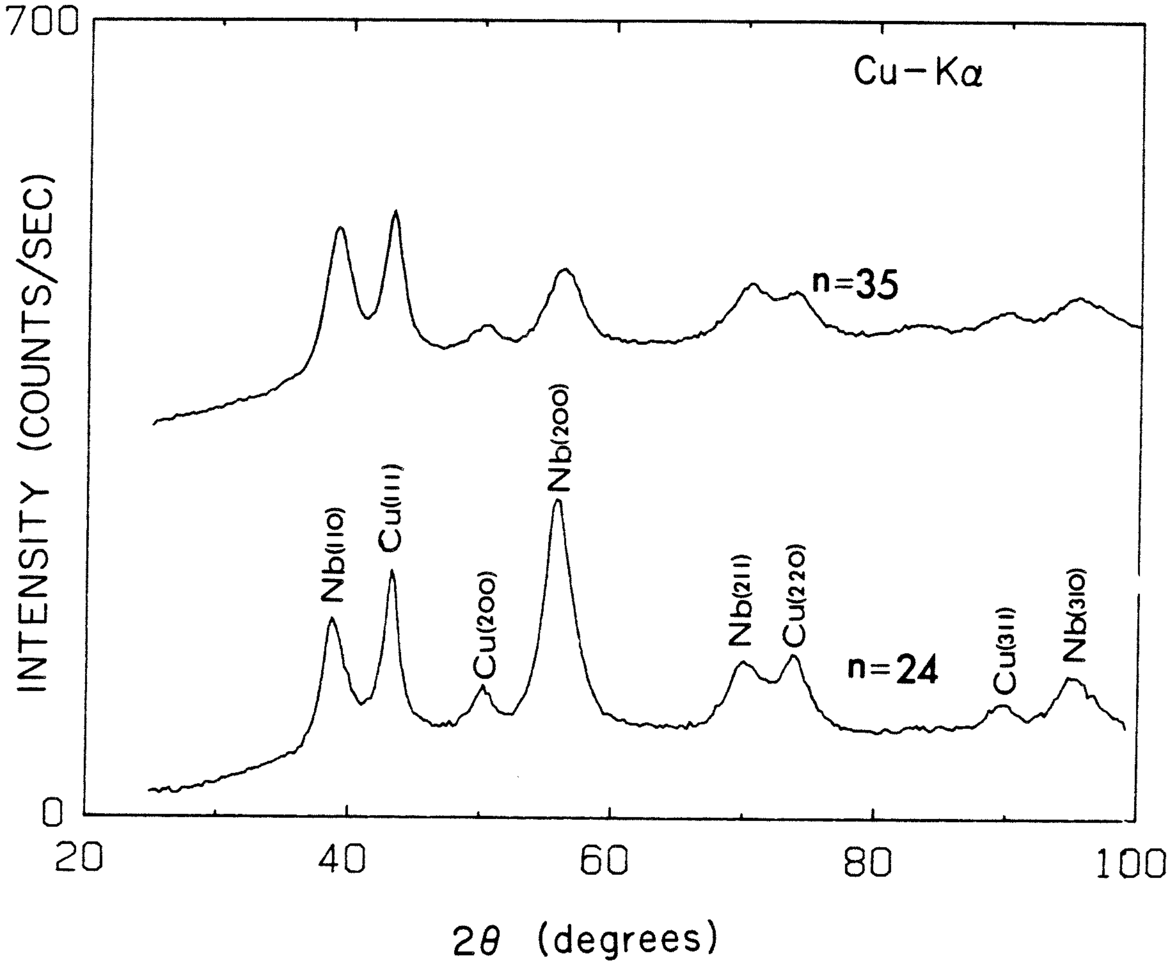

Figure 3.20 X-ray scattering intensity as a function of scattering angle for a crystalline $Cu_{75}Nb_{25}$ composite at different numbers of deformation passes n.

4. SOLID-STATE REACTIONS BETWEEN CRYSTALLINE AND AMORPHOUS PHASES

4.1 INTRODUCTION

An interesting aspect of solid- state amorphization reactions is the reaction of an amorphous alloy $A_{1-x}B_x$ with the pure metal B. Fig. 4.1 illustrates the Gibbs free energies of the terminal solid solutions and the amorphous alloy in the binary system Au-Y, and the dotted line represents the free energy of a mixture of amorphous $Au_{20}Y_{80}$ with pure gold. According to the common tangent rule, there is a thermodynamic driving force for gold to mix with the amorphous phase for compositions $x_0 < x < 1$, and the maximum attainable gold concentration is x_0. Here again, we assume that the formation of crystalline compounds is kinetically bypassed.

Such amorphous- crystalline reactions can be used to study self-diffusion in an amorphous alloy, i.e., the diffusion of one of its components, as opposed to an impurity diffusion. All published data[4.2] on diffusion in amorphous alloys are concerned with tracer diffusion. In self- diffusion, the background signal is high due to the high concentration of the diffusing species, and it introduces statistical noise into the concentration measurement, making the measurement more difficult.

In the following section, several experimental results will be described for crystalline- amorphous reactions in thin films as well as in bulk composites.

4.2 EXPERIMENTAL RESULTS

4.2.1 Thin Film Reactions

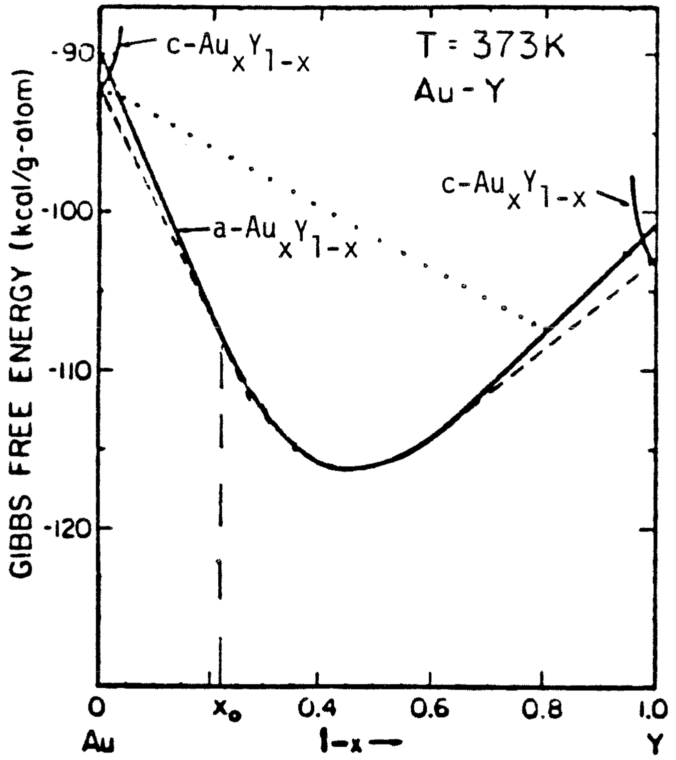

Figure 4.1 Gibbs free energy as a function of composition for the binary system Au_xY_{1-x} (from Ref. 4.1). The solid lines denote the amorphous phase and the terminal solid solutions, and the dotted line represents a mixture of a-$Au_{20}Y_{80}$ with pure gold.

Multilayered films were prepared with alternating a-Au_xY_{1-x} and Au layers and also a-Au_yLa_{1-y} and Au. The thickness of the layers was 200-2000 Å and a total of 6-8 layers were deposited each time. Fig. 4.2 shows the X-ray diffraction pattern for alternating layers of $Au_{34}La_{66}$ (1000 Å each) and Au (200 Å each) before and after reaction at 80 °C for 4 hours. It can be seen that a major fraction of the gold dissolved in the amorphous alloy. In Fig. 4.3 , a similar pattern is shown for multilayers of $Au_{40}Y_{60}$ (≃600 Å each) and Au (≃125 Å each), reacted for 5 hours at 102 °C. All but a small trace of gold is dissolved, producing an amorphous alloy of the composition $Au_{57}Y_{43}$. Fig. 4.4 shows the Rutherford backscattering spectra for a reaction of a bilayer of $Au_{42}Y_{58}$ and Au at 96 °C for 5.5 hours. One can see how the sharp step in the composition becomes less steep as the gold diffuses into the amorphous phase.

4.2.2 Reactions in Bulk Composites

An experiment similar to the above was conducted with bulk materials. Composites were prepared from amorphous $Zr_{67}Ni_{33}$ foils produced in the "piston and anvil" and nickel foils, according to the method described in Chapter 2. The total number of deformation passes was 11, and the average composition of the samples was 48- 60 atomic percent nickel. Fig. 4.5 shows the X-ray diffraction for a composite with an average composition of $Zr_{52}Ni_{48}$, as rolled and after reaction for 19 days at 275 °C. It is apparent that most of the nickel dissolved into the amorphous phase and that the broad peak shifted due to the change in composition from 37 to 41 degrees (for Cu K_α radiation).

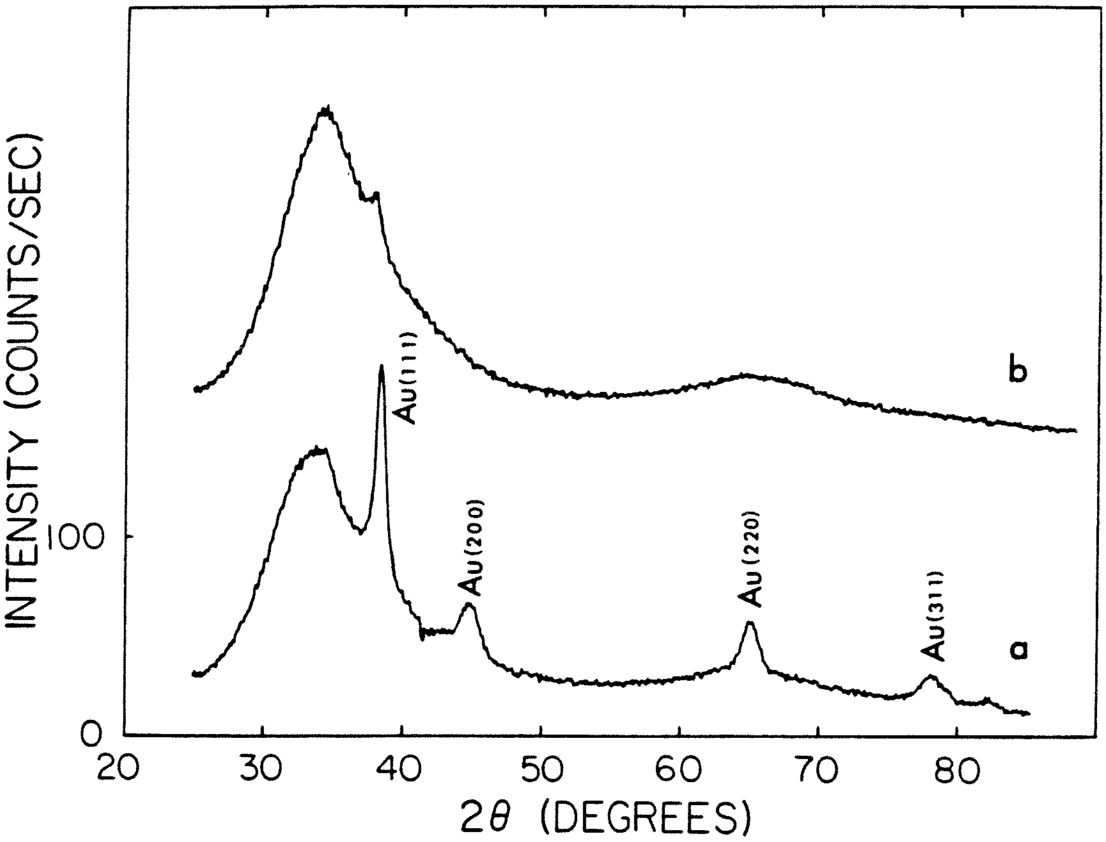

Figure 4.2 X-ray scattering intensity as a function of scattering angle for alternating layers of a-$Au_{34}La_{66}$ and Au: a) as deposited, b) reacted at 80 °C for 4 hr.

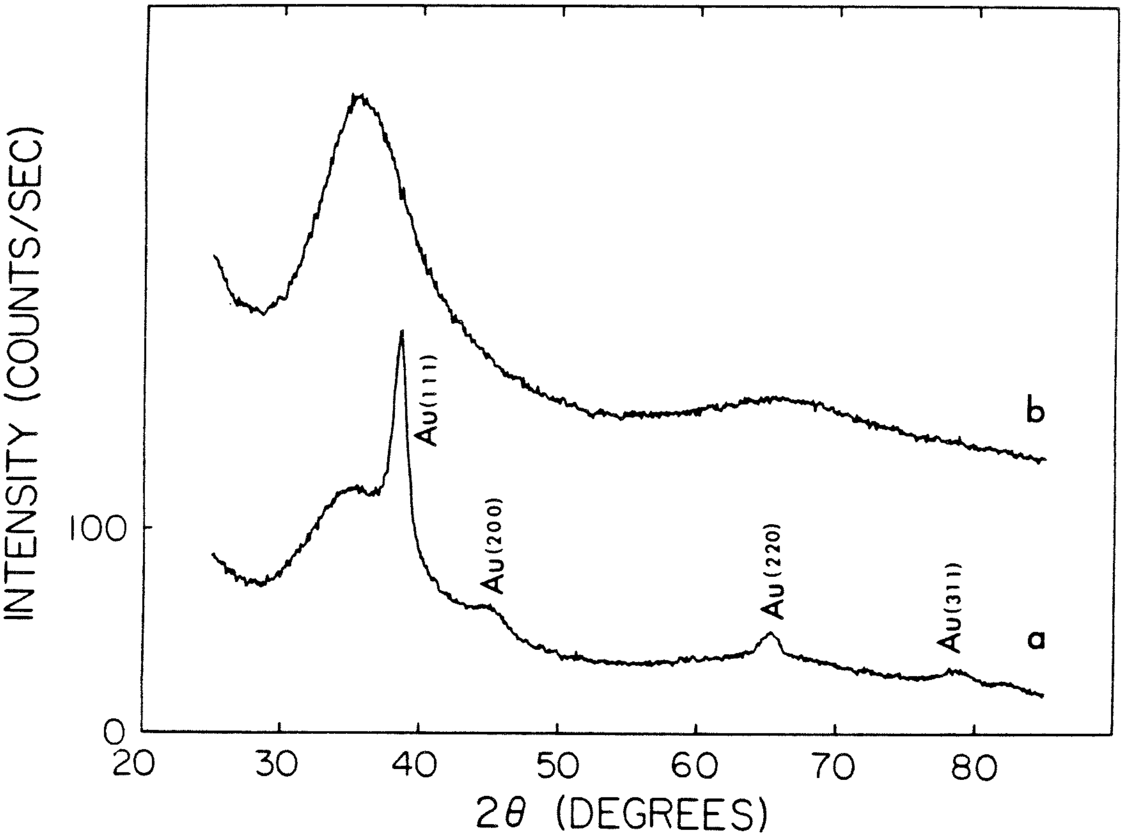

Figure 4.3 X-ray scattering intensity as a function of scattering angle for alternating layers of a-$Au_{40}Y_{60}$ and Au: a) as deposited, b) reacted at 102 °C for 5 hr.

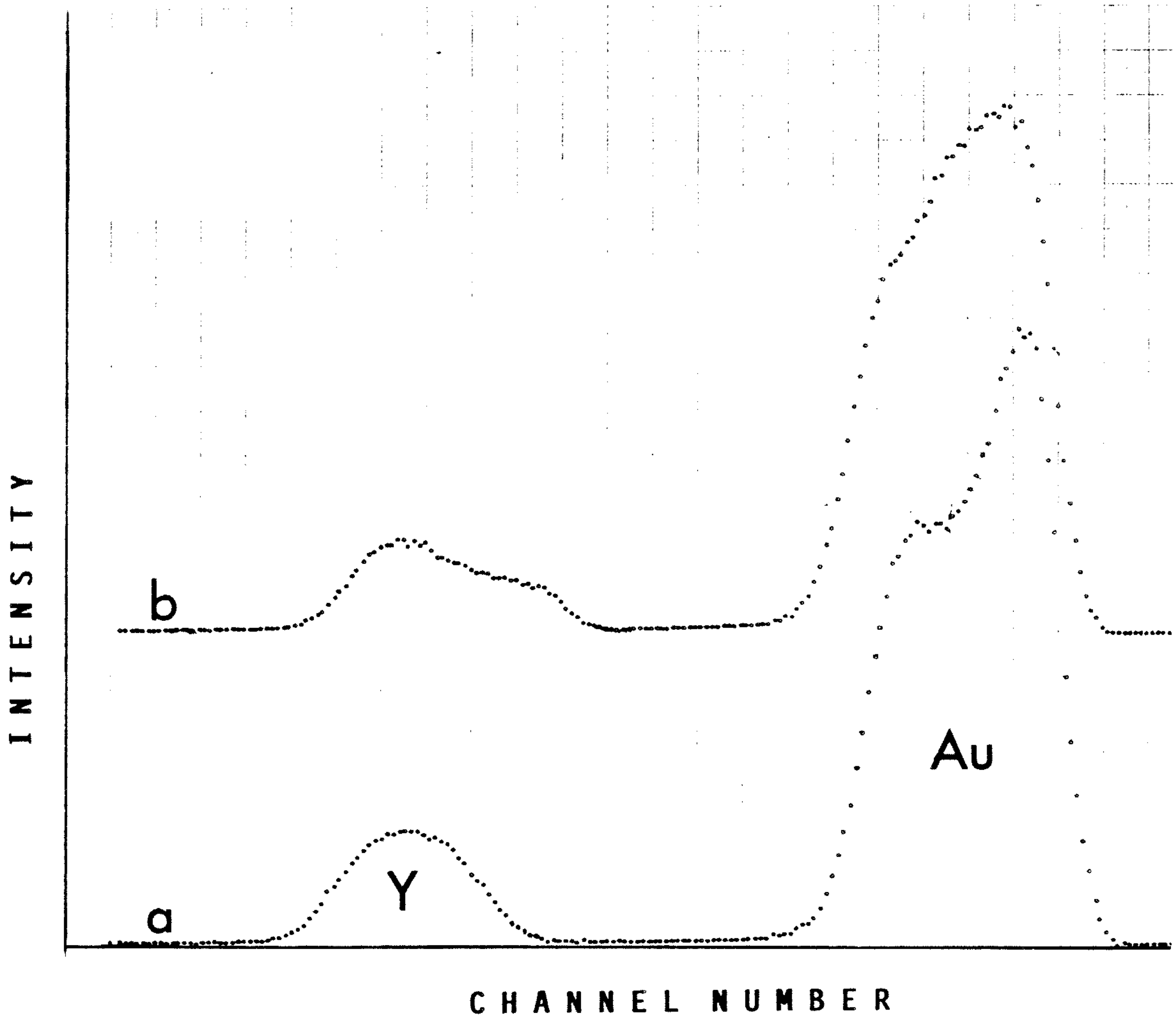

Figure 4.4 Backscattering of a bilayer of $Au_{42}Y_{58}$ and Au: a) as deposited, b) reacted at 96 °C for 5.5 hr.

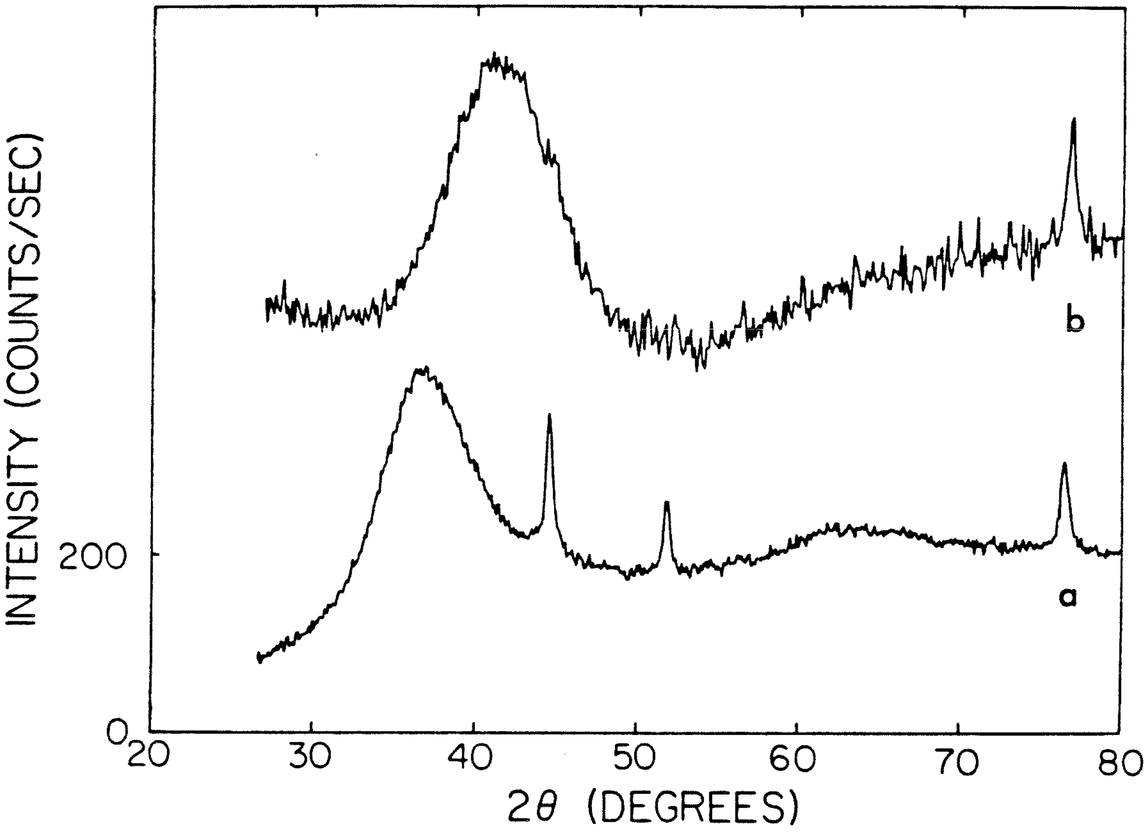

Figure 4.5 X-ray scattering intensity as a function of scattering angle for a composite a-Zr_2Ni - Ni sample with an average composition $Zr_{52}Ni_{48}$: a) as rolled, b) reacted for 19 days at 275 °C.

4.3 DISCUSSION

The above experiment can serve for a rough estimate of the diffusion coefficients governing the amorphous- crystalline reaction. In the case of Au-Y, an almost complete reaction was observed by X-ray diffraction. Based on previous results for solid- state amorphization,[4.3,4.4] we assume diffusion controlled growth of the amorphous layer. If one ignores the change of total volume upon alloying, the thickness of the added amorphous layer is equal to the thickness of the gold layer before reaction. Since each gold layer reacts at its two interfaces, the thickness of each added amorphous layer is half that of the gold. We have the thickness x = 60 Å, the duration t = 5h = 18000 sec (this is an upper limit for the diffusion time, since the sample was scanned only after 5 hours of reaction). One obtains:

$$D = x^2/t = 2*10^{-17}\ \mathrm{cm}^2/\mathrm{sec} = 2*10^{-21}\ \mathrm{m}^2/\mathrm{sec}\ . \qquad (4.1)$$

Cantor[4.5] has shown, that for gold diffusion in several metallic glasses, one obtains all points on an Arrhenius plot roughly on one line, if the temperature is normalized by the glass-transition temperature T_g for each alloy. For the above case, T_g can be estimated from a resistivity measurement performed by Schwarz et al.[4.1] for a-$Au_{40}Y_{60}$. Fig. 4.6 shows Cantor's plot with our estimated data point added to it. For the given temperature, the point lies within the range defined by previous points, if one considers the fact that the diffusion time was overestimated (i.e., the diffusion coefficient underestimated).

The results presented here are only preliminary, and it is

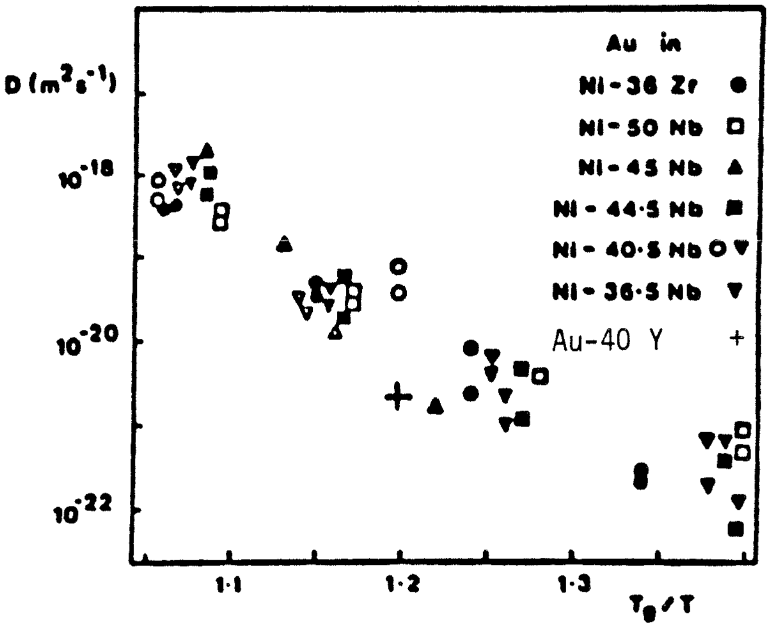

Figure 4.6 Au diffusion coefficients in metal- metal amorphous alloys (from Ref. 4.5). "+" denotes our data point.

worthwile to perform a complete experiment to determine the diffusion coefficients involved in the reaction and their temperature and composition dependence. For a small amount of material diffusing into the amorphous phase, its composition can be assumed constant and the diffusion data can be analyzed with Darken's equation and the regular solution approximation. However, some important insight into SSR can be gained from the above observations. In a recent publication, Barbour et al.[4.6] claimed that the diffusion during a solid- state growth of an amorphous layer has to go through short circuits, e.g., the "memory" of grain boundaries from the original crystalline material. They argue that there can be no bulk diffusion in the amorphous phase because it would lead to crystallization. This claim is based on Buschow[4.7,4.8] who interpreted the crystallization behavior of Zr, Hf and rare-earth-based metallic glasses as diffusion-limited, and showed that the crystallization temperature T_x of these glasses scales with the enthalpy of formation of a hole corresponding to the smaller atomic species. If we assume the amorphous thin films in the above experiment to be uniform, then the results prove that there is indeed bulk diffusion in the amorphous phase. (The assumption of uniformity is usually justified for amorphous co- deposited films, and the formation of islands during deposition is generally observed only for crystalline materials.) A possible explanation is that the crystallization is not simply explainable as diffusion-limited. In fact, Shikhmanter et al.[4.9] show that polymorphic crystallization of amorphous CuEr occurs by (diffusionless) nucleation and growth, and the activation energy for the atomic migration across the interface is equal to the enthalpy of formation of a vacancy in a copper site. This indicates that the fact that T_x scales with the the enthalpy of hole formation does not necessarily lead to the conclusion that the crystallization is diffusion- limited, but rather probably has a more fundamental explanation. The crystallization requires correlated motion of both species to form the right configuration for the crystalline unit- cell, and diffusion of one species does not lead to crystallization.

The considerable shift in the Bragg-peak position for the Ni-Zr_2Ni reaction is a result of the change of the composition of the amorphous phase. As the atoms of the smaller species diffuse into the amorphous phase, the average interatomic distance decreases; i.e., the position of the maximum goes to higher K- values or angles. If we compare the peak position after reaction - 41 ° or 2.86 $Å^{-1}$ - to the values reported by Buschow[4.10] for a series of Ni_xZr_{1-x} alloys, the final product should contain 63 atomic percent nickel. This is obviosly impossible because the average composition of the composite was 48 atomic percent nickel. This could be a result of the inhomogeneity of the reaction product.

It is worth mentioning a possible practical application of the reaction between crystalline and amorphous phases. In an effort to produce amorphous alloys in bulk form, attempts to consolidate amorphous metal powders under hydrostatic pressure were not successful because the powder particles did not bond. Adding a small amount of one of the chemical species in the alloy could possibly provide a "glue" for diffusional bonding.

5. CONCLUSION

5.1 SUMMARY

It has been demonstrated for the first time that solid-state reactions can be used to synthesize bulk amorphous alloys. This result has potential use for practical applications of amorphous alloys, when bulk material is needed. In the present work, new characterization techniques have been used which were not applicable to previously synthesized solid-state reacted thin film alloys.

As for previously studied thin film samples, amorphization could be induced by thermal reaction. In addition, for sufficiently ductile elemental components, a complete reaction was achieved by extensive rolling near room temperature. Like the reaction by thermal treatment, this reaction was found to be driven by chemical driving forces.

The crystallization behavior of the alloys formed, as studied by DSC, was very similar to that of the corresponding alloys prepared by more conventional methods. The atomic-scale structure, as measured by X-ray diffraction, also showed very good agreement between the alloys. One can conclude that the (metallic) glassy state is well defined and not a kinetically "trapped" unstable state. The glass is essentially the same, whether formed by cooling from the vapor or liquid (see Ref. 5.1) or by solid-state reaction.

The amorphous-crystalline reactions described in Chapter 4 show that there is indeed bulk self-diffusion in Au-Y glass without crystallization. Amorphization by solid-state reaction does not need to be explained by short-circuit diffusion paths.

5.2 SUGGESTIONS FOR FUTURE RESEARCH

Many questions regarding the mechanism of amorphization by solid-state reactions are still open. For most of them, providing the answer will require sophisticated experimental techniques and/or extensive investment in time and effort. One can expect that many questions will be answered within several years.

Throughout this thesis, information concerning the morphology of the composite was gained by indirect evidence, such as X-ray diffraction. Transmission electron microscopy (TEM) could provide a tool for directly monitoring the layered structure of the composite. Furthermore, TEM could be used to observe the amorphization process in a single microcrystal in real time. It could answer the question as to whether the amorphization is preceded by supersaturation of the crystalline host lattice.

The suggested effect of strain in enhancing the reaction rate can be studied by monitoring the rate of reaction as a function of directly applied compressive or shear stresses.

The difference observed in the composition of the amorphous phases formed in the Ni-Er and Cu-Er composites suggests differences in the driving forces between the systems. The free-energy curves for the two systems must have different shapes. This implies that the regular solution model is not sufficient for describing the free energies of the amorphous phases. DSC measurements of the enthalpies of mixing involved would give direct data upon which free energy diagrams could be based. This would provide a basis for a more rigorous evaluation of the theoretical attempts (e.g. , Miedema[5.2]) at describing the alloy enthalpies. A complete understanding of alloy mixing enthalpies would require a full understanding of the electronic structure of the alloy. A first principles theory of alloying will therefore remain a difficult objective.

The presence of defects, such as interfaces, dislocations and point defects, causes a rise in the free-energy of the crystalline phases. Thus, the crystalline phases become thermodynamically less favorable than the amorphous alloys in a composition range extended beyond that indicated by the (metastable) equilibrium free energy diagram. In other words, defects cause the crystalline phases to be in a superheated state. This issue can be addressed by studying the range of composition in which amorphous phases form as a function of the defect concentration. The defect concentration can be controlled by varying the layer thicknesses and the deposition conditions and by causing radiation damage. However, one has to keep in mind that defects will affect the reaction kinetics.

REFERENCES

Chapter 1

1.1. W. Buckel, R. Hilsch, Z. Phys **138**, 109 (1954).

1.2. W. Klement, R. H. Willens, P. Duwez, Nature **187**, 869 (1960).

1.3 B. P. Dolgin, Ph. D. Thesis, California Institute of Technology, 1984.

1.4 Topics in Applied Physics, Vol. 46: Glassy Metals I (Springer Verlag, 1981), 1982.

1.5 N. Bloembergen, in: Laser-Solid interactions and Laser Processing, eds. S.D. Ferris, H.J. Leamy and J.M. Poate (Academic Press, New York, 1979) p.1.

1.6 H. H. Liebermann, in Amorphous Metallic Alloys, ed. F. E. Luborsky (Butterworths Monographs in Materials, 1983).

1.7 M. G. Scott, in Ref. 1.6, p. 144.

1.8 J. W. Christian, in: Physical Metallurgy, editor R.W. Cahn (North Holland, 1970), p.481.

1.9 M. H. Cohen and D. Turnbull, Nature **189**, 131 (1961).

1.10 X. L. Yeh, K. Samwer and W. L. Johnson, Appl. Phys. Lett. **42** 242 (1983).

1.11 R. B. Schwarz and W. L. Johnson, Phys. Rev. Lett. **51**, 415 (1983).

1.12 D. Turnbull, Contemp. Phys. **10**, 473 (1969).

1.13 A. R. Miedema, in Philips Technical review **36**, No. 8 (1976), p. 217.

1.14 W. L. Johnson, B. P. Dolgin and M. Van Rossum, in Glass... Current Issues, ed. A. F. Wright and J. Dupuy, Nato ASI Series, Series E 92 (Martinus Nijhof, Dortrecht 1985).

1.15 M. Van Rossum, M.-A. Nicolet and W. L. Johnson, Phys. Rev. **B29**, 5498 (1984).

1.16 B. M. Clemens, W. L. Johnson and R. B. Schwarz, J. Non-Cryst. Sol. **61&62**, 817 (1984).

1.17 M. Atzmon, J. D. Verhoeven, E. D. Gibson and W. L. Johnson, Appl. Phys. Lett. **45**, 1052 (1984).

1.18 K. Samwer, A. Regenbrecht and H. Schröder, in Rapidly Quenched Metals, eds. S. Steeb and H. Warlimont (North Holland, 1985), p. 1577.

1.19 E. J. Cotts and S. H.-C. Kong, private communication.

1.20 R. B. Schwarz, K. L. Wong, W. L. Johnson and B.M. Clemens, J. Non-Cryst. Sol. **61&62**, 129 (1984).

1.21 M. Atzmon and W. L. Johnson, present thesis.

1.22 H. Schröder, K. Samwer and U. Köster, Phys. Rev. Lett. **54**, 197 (1985).

1.23 J. W. Christian, The Theory of Transformations in Metals and Alloys (Pergamon Press, 1965), p. 362.

1.24 L. Schultz, in: Amorphous Metals and Non-Equilibrium Processing, ed. M. von Allmen (Les Editions de Physique, Les Ulis, 1984).

1.25 K. M. Unruh, W. J. Meng, W. L. Johnson, A. P. Thakoor and S. K. Khanna, Mat. Res. Soc. Symp. Proc. **37**, 551 (Boston, 1984).

1.26 A. C. Wright, A. C. Hannon, R. N. Sinclair, W. L. Johnson and M. Atzmon, J. Phys. F: Met. Phys **14** (1984).

1.27 G. S. Cargill, J. Appl. Phys. **41**, 12 (1970).

1.28 J. D. Bernal, Nature (London) **183**, 141 (1959).

1.29 L. von Heimendall, J. Phys. F: Met. Phys. **5**, L141 (1975) and J. A. Barker, J. L. Finney and M. R. Hoare, Nature **257**, 120 (1975).

1.30 J. F. Sadoc, J. Dixmier, A. Guinier, J. Non-Cryst. Sol. **12**, 46 (1973).

1.31 G. S. Cargill, in Solid State Physics , Vol. 30, eds. H. Ehrenreich, F. Seitz and D. Turnbull (Academic Press, 1975).

1.32 H. Schmalzried, Solid State Reactions (Verlag Chemie, Weinheim/ Bergstr., 1974, Academaic Press, New York and London) p.53.

1.33 L. S. Darken, Am. Inst. Mining Met. Engrs. Inst. Met. Div. Metals Technol. 15, Technol. Publ. 2311 (1948), 2443 (1948).

1.34 J. W. Cahn, Trans. Met. Soc. AIME **242**, 166 (1968).

1.35 C. P. Flynn, Point Deffects and Diffusion (Clarendon Press, Oxford, 1972) p. 15.

1.36 H. P. Wahl, G. Wassermann, Z. Metallk. **61**(4), 326 (1970).

1.37 A. C. Sacharoff, R. M. Westervelt and J. Bevk, Phys. Rev. **B15**, Rapid Comm. 26(10), 5976 (1982).

1.38 J. Bevk, in Annual Review of Materials Science, eds. R. A. Huggins, R. H. Bubbe and D. A. Velmilyea (Annual Review Inc., Palo Alto, 1983), Vol. 13.

1.39 J. Bevk, J. P. Harbison, and J.L. Bell, J. Appl. Phys. **49**, 6031 (1978).

1.40 G. Frommeyer and G. Wasseremann, Acta Metal. **23**, 1353 (1975).

Chapter 2

2.1 M. Atzmon, J. D. Verhoeven, E. D. Gibson and W. L. Johnson, Appl. Phys. Lett. **45**, 1052 (1984).

2.2 G. E. Dieter, Mechanical Metallurgy (McGraw Hill International, 1981), p. 533.

2.3 B. P. Dolgin, Ph.D. Thesis, California Institute of Technology (1984).

2.4 W. Klement, R. H. Willens and P. Duwez, Nature **187**, 869 (1960).

2.5 C. S. Barrett, T. B. Massalaki, Structure of Metals (McGraw Hill, 1966), p. 130.

2.6 H. A. Klug and L. E. Alexander, X-ray Diffraction Procedures, (John Wiley & Sons, New York 1974), p. 355.

2.7 D. T. Chromer and J. T. Waber, Acta Cryst. **18**, 104 (1965).

2.8 D. T. Chromer, Acta Cryst. **18**, 17 (1965).

2.9 D. T. Chromer and J. B. Mann, J. Chem. Phys. **47**, 1892 (1967).

2.10 D. T. Chromer, J. Chem. Phys. **50**, 4857 (1969).

2.11 A. R. Williams, Ph.D. Thesis, California Institute of Technology (1981).

2.12 J. L. McNaughton and C. T. Mortimer, in IRS; Physical Chemistry Series 2, Vol. 10 (Butterworths, London 1975).

Chapter 3

3.1 B. M. Clemens, W. L. Johnson and R. B. Schwarz J. Non- Cryst. Sol. **61&62**, 817 (1983).

3.2 A. K. Niessen, F. R. de Boer, R. Boom, P. F. de Châtel, W. C. M. Mattens and A. R. Miedema, Calphad **7**, 51 (1983).

3.3 O. J. Kleppa and S. Watanabe, Met. Trans. 13B, 391 (1982).

3.4 I. V. Nikolaenko, E. A. Beloborodova, G. I. Batalin, N. I. Frumina and V. S. Zhuravlev, Russ. J. of Phys. Chem. 57, 1897 (1983).

3.5 A. R. Miedema, in Philips Technical Review 36, No. 8, 217 (1976).

3.6 S. Barett and T. B. Massalasky, Structure of Metals (Pergamon, Oxford, 1980), p. 555.

3.7 Friedel, Dislocations (Pergamon Press, 1964), p. 418.

3.8 A. Guinier, X-Ray Diffraction (W. H. Freeman and Co., San Francisco 1963), p. 124.

3.9 S. F. Bartram, in Handbook of X-Rays, ed. E. F. Kaelble (McGraw Hill, 1967), p. 17-1.

3.10 M. G. Scott, in Amorphous Metallic Alloys, ed. F. E. Luborsky (Butterworth, London 1983), p. 160.

3.11 B. P. Dolgin, Ph.D. Thesis, California Institute of Technology, 1984.

3.12 F. A. Shunk, Constitution of Binary Alloys, 2nd Suppl. (McGraw Hill, New York, 1969).

3.13 Y. D. Dong, G. Gregan and M. G. Scott, J. Non-Cryst. Sol. 43,403 (1981)

3.14 A. J. Kerns, D. E. Polk, R. Ray and B. C. Giessen, Mater. Sci. Eng. 38,49 (1979).

3.15 M. Mehra, W. L. Johnson, A. P. Thakoor and S. K. Khanna, Sol. St. Comm. 47, 859, 1983.

3.16 J. Mathews and R. L. Walker, Mathematical Methods of Physics (Benjamin Cummings Publ. Co., 1964), p. 243.

3.17 G. E. Dieter, Mechanical Metallurgy (McGraw Hill International, 1981), pp. 121-122.

3.18 Metals Handbook, Vol. 1, ed. T. Lyman (Amreican Society for Metals, 1961), p. 544.

3.19 R. H. Willens, A. Kornblit, L. R. Testardi and S. Nakahara, Phys. Rev. B 25, 290 (1982).

3.20 A. Cottrell, An Introduction to Metallurgy (Edward Arnold, London 1975) p. 341.

3.21 R. A. Swalin, Thermodynamics of Solids (John Wiley, New York, 1972), p. 145.

Chapter 4

4.1 R. B. Schwarz, K. L. Wong, W. L. Johnson and B. M. Clemens, J. Non- Cryst. Sol. **61&62**, 129 (1984).

4.2 A review of diffusion in metallic glasses is given by: B. Cantor and R. W. Cahn, in Amorphous Metallic Alloys, ed. F. E. Luborsky (Butterworths, 1983), p. 487.

4.3 M. Van Rossum, M-A. Nicolet and W. L. Johnson, Phys. Rev. **B 29**, 5498 (1984).

4.4 See Ref. 1.25.

4.5 B. Cantor, in Rapidly Quenched Metals, eds. S.Steeb and H. Warlimont (North Holland, 1985), p. 595.

4.6 J. C. Barbour, F. W. Saris, M. Nastasi and J. W. Mayer, Phys. Rev. **B 32**, 1363 (1985).

4.7 K. H. J. Buschow, J. Appl. Phys. **52**, 3319 (1981).

4.8 K. H. J. Buschow and N. M. Beekmans, Phys. Rev. **B 19**, 3843 (1979).

4.9 L. Shikhmanter, M. Talianker and M. P. Dariel, J. Phys. Chem. Solids **44**, 745 (1983).

4.10 K. H. J. Buschow, J. Phys. F: Met. Phys. **14**, 593 (1984).

Chapter 5

5.1 See Ref. 3.15.

5.2 See Ref. 3.5.

APPENDIX: LIST OF PUBLICATIONS

1) Atzmon M. and W. L. Johnson, A Cooling-Rate Dependent Structure of Amorphous $(Au_xCu_{1-x})_{91}La_9$, Journal of Non-Crystalline Solids **55**, 395 (1983). Presented at the March Meeting of the American Physical Society, 1983, Los Angeles, California.

2) Williams A. R., J. Eckert, X. L. Yeh, M. Atzmon and K. Samwer, Inelastic Neutron Scattering from Amorphous Hydride of Zr_2Pd, Fifth International Conference on Liquid and Amorphous Metals, Los Angeles, California, Journal of Non-Crystalline Solids **61&62**, 643 (1984).

3) Wright A. C., A. C. Hannon, R. N. Sinclair, W. L. Johnson and M. Atzmon, The Neutron Diffraction Double Null Isotopic Substitution Technique, Journal of Physics F: Metal Physics **14**, L201 (1984).

4) Atzmon M., J. D. Verhoeven, E. D. Gibson and W. L. Johnson, Formation and Growth of Amorphous Phases by Solid-State Reaction in Elemental Composites Prepared by Cold-Working, Applied Physics Letters **45**, 1052 (1984).

5) Atzmon M, J. D. Verhoeven, E. D. Gibson and W. L. Johnson, Study of Amorphous Phases Formed by Solid-State Reaction in Elemental Composites, Fifth International Conference on Rapidly Quenched Metals, Würzburg, W. Germany, 1984, in "Rapidly Quenched Metals," eds. S. Steeb and H. Warlimont (North Holland, Amsterdam 1985), p. 1561.

6) Maret M., P. Chieux, P. Hichter, M. Atzmon and W. L. Johnson, Short-Range Order in $Ni_{33}Y_{67}$ and $Cu_{33}Y_{67}$ Amorphous Ribbons, in Fifth International Conference on Rapidly Quenched Metals, Würzburg, W. Germany, 1984, in "Rapidly Quenched Metals," eds. S. Steeb and H. Warlimont (North Holland, Amsterdam 1985), p. 521.

7) Johnson W. L., M. Atzmon, M. Van Rossum, B. P. Dolgin and X. L. Yeh, invited paper at the Fifth International Conference on Rapidly Quenched Metals, Würzburg, W. Germany, 1984, in "Rapidly Quenched Metals," eds. S. Steeb and H. Warlimont (North Holland, Amsterdam 1985), p. 1515.

8) Wright A. C., A. C. Hannon, A. G. Claire, R. N. Sinclair, W. L. Johnson and M. Atzmon, The Atomic and Magnetic Structure of Amorphous Dy_7Ni_3, Third International Conference on the Structure of Non-Crystalline Materials, Grenoble, 1985.

9) Atzmon M., K. M. Unruh and W. L. Johnson, Formation and Characterization of Amorphous Erbium-Based Alloys Prepared by Near-Isothermal Cold-Rolling of Elemental Composites, to be published in Journal of Applied Physics.

10) Johnson W. L., X. L. Yeh and M. Atzmon, Metallic Glass Formation by Solid-State Diffusion Reactions, EPRI - Acta Metallurgica Workshop on Amorphous Metals and Semiconductors, San Diego, California 1985, to be published in *Acta Metallurgica*.

11) Atzmon M., K. M. Unruh and W. L. Johnson, Study of Amorphous Erbium-Based Alloys Formed by Near-Isothermal Cold-Rolling of Elemental Composites, to be presented at the Fall Meeting of the Materials Research Society, Boston ,1985.